New Research Proposal to Jefferson Lab PAC 20

Deeply Virtual Compton Scattering with CLAS at 6 GeV

D. Doughty, L. Elouadrhiri[1], S. Stepanyan[1,2]
Christopher Newport University and Jefferson Lab, Newport News, VA 23606, USA

H. Avakian, S. Boyarinov, V.D. Burkert[1], D. Cords, M. Ito, K. Joo,
Yu. Sharabian, E. Smith
Jefferson Lab, Newport News, VA 23606, USA

J. Ball, D. Doré, M. Garçon[1], J.-M. Laget, L. Morand, F. Sabatié
DAPNIA/SPhN, CEA-Saclay, F-91191 Gif-sur-Yvette, France

S. Bouchigny, J.-P. Didelez, M. Guidal, C. Hadjidakis, E. Hourany
Institut de Physique Nucléaire, F-91406 Orsay, France

S. Kuleshov, O. Pogorelko, P. Shiskov
Institute of Theoretical and Experimental Physics, Moscow, 117259, Russia

H. Aznauryan, N. Dashyan, K. Egiyan
Yerevan Physics Institute, Yerevan, Armenia 375036

P. Stoler
Rensselaer Polytechnic Institute, Troy, NY 12181, USA

G. Dodge, C.E. Hyde-Wright, S.E. Kuhn, A. Radyushkin, L. Weinstein
Old Dominion University, Norfolk, VA 23529, USA

D. Carman
Ohio University, Athens, OH 45701, USA

M. Vanderhaeghen
Johannes Gutenberg Universität, Mainz, Germany

[2]Contact person
[1]Co-spokesperson

Abstract

We propose to study Deep Virtual Compton Scattering (DVCS) using the CEBAF 6 GeV polarized electron beam and the CLAS detector at Jefferson Lab. The main focus of the experiment will be measurement of the beam spin asymmetry in the reaction $\vec{e}p \rightarrow ep\gamma$. This asymmetry is directly proportional to the imaginary part of the DVCS amplitude and gives access to a combination of the Generalized Parton Distributions H, E, $\tilde{H}$, and $\tilde{E}$. The Q^2, x_B and t dependence of the DVCS amplitude will be studied in a wide range of kinematics. In addition, helicity-dependent cross section differences will be measured. In some kinematics, we will be able to determine the unpolarized DVCS cross section by subtracting the Bethe-Heitler contribution. 60 days of new beam time are requested for this experiment. In addition, we ask for approval to run with the standard CLAS configuration concurrently with the E1-6 run group, scheduled for the fall of 2001.

Contents

1 Introduction **4**

2 Theory and motivation **5**
2.1 Phenomenology of the GPDs 5
2.2 Deeply Virtual Compton Scattering 7

3 Experimental situation **11**
3.1 Recent evidence from JLab with CLAS 11
3.2 JLab proposals 12
3.2.1 Hall B - E99-105 12
3.2.2 Hall A - E00-110 12
3.3 Experiments at HERA 12
3.3.1 HERMES 12
3.3.2 H1 and ZEUS experiments 13
3.4 CERN experiment 13

4 A dedicated DVCS experiment in Hall B **14**
4.1 An optimized CLAS configuration 14
4.1.1 A solenoidal shielding magnet for Møller electrons 15
4.1.2 A photon detector for small angle coverage 19
4.1.3 Trigger and data acquisition 22
4.1.4 Calibration 22
4.2 Event identification, reconstruction, acceptances 22
4.2.1 Separation of single γ from $\gamma\gamma$ events. 23
4.3 Count rates and statistical errors 25
4.4 Systematic errors 27
4.5 Projected results and comparison to models 28

5 Data taking during the E1-6 run **29**

6 Summary and beam time request **29**

1 Introduction

Much of the internal structure of the nucleon has been revealed during the past three decades through the inclusive scattering of high-energy leptons on nucleons in the Bjorken -or "Deep Inelastic Scattering" (DIS)- regime. Simple theoretical interpretations of the experimental results and quantitative conclusions can be reached in the framework of the parton model and QCD when one sums over all possible hadronic final states. For instance, *unpolarized* DIS led to the discovery of the quark and gluon substructure of the nucleon, with the quarks carrying about half of the nucleon's momentum. Furthermore, *polarized* DIS revealed that only about 25% of the spin of the nucleon is carried by the quark intrinsic spin. However, very little is known about quark-quark correlations, the transverse quark momentum distribution, and contributions of correlated quark-antiquark pairs (mesons) to the nucleon wave function.

The recently developed formalism of "Generalized Parton Distributions" (GPDs) [1, 2] showed that such information can be obtained in hard exclusive leptoproduction experiments. The GPDs contain information on the interference between different quark configurations, on the quark transverse momentum distribution, as well as their angular momentum distribution. GPDs provide a unifying picture for an entire set of fundamental quantities of hadronic structure, such as: the vector and axial vector nucleon form factors, the polarized and unpolarized parton distributions, and the spin components of the nucleon due to orbital excitations.

Deeply Virtual Compton Scattering (DVCS) is one of the key reactions to determine the GPDs experimentally, and it is the simplest process that can be described in terms of GPDs. We propose a measurement of DVCS in Hall B at Jefferson Lab with a 6 GeV longitudinally polarized electron beam, with a CLAS configuration optimized for running with higher luminosity, 2×10^{34} cm^{-2}s^{-1}, and with a larger acceptance for photon detection.

The first experimental observation of DVCS was obtained from our recent analysis of CLAS data with a 4.2 GeV polarized electron beam in a limited kinematical regime around $Q^2 = 1.5$ GeV^2 and $x_B = 0.22$ [3]. The new measurements will map out the DVCS amplitude in the range of Q^2 from 1 to 4 GeV^2, and x_B from 0.15 to 0.55. The main goal will be a study of the x_B and t dependence of the beam spin asymmetry. These measurements are essential for the study of GPDs.

The CLAS detector with the proposed new configuration and a 6 GeV longitudinally polarized electron beam form a unique facility to perform such measurements with a single experimental setup in a wide range of kinematics.

2 Theory and motivation

2.1 Phenomenology of the GPDs

We briefly review in this section the formalism of the Generalized Parton Distributions. In recent years, Ji [1] and Radyushkin [2] (see also Ref. [4]) have shown that the deeply virtual Compton scattering (DVCS) amplitude in the forward direction can be factorized in leading-order pQCD into a hard-scattering part (exactly calculable in pQCD) and a non-perturbative nucleon structure part, as illustrated in Fig. 1a. In these so-called "handbag" diagrams, the lower blob represents the soft structure of the nucleon, and can be described in terms of four structure functions, known as the GPDs.

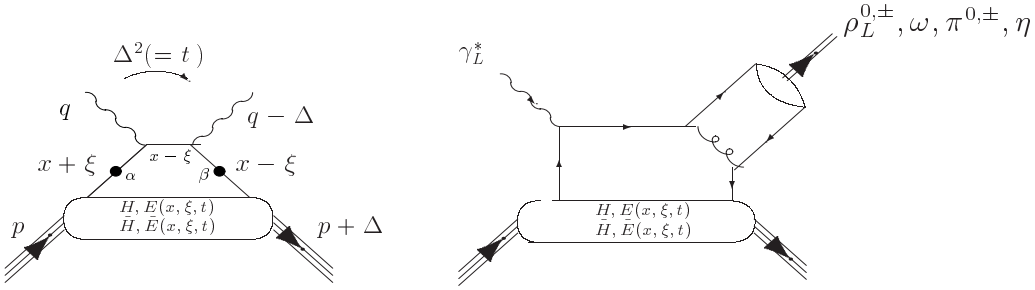

Figure 1: "Handbag" diagrams for (a) DVCS (left) and (b) meson production (right).

There are 4 independent GPDs: $H, \tilde{H}, E$, and $\tilde{E}$; they depend upon three kinematic variables: x, ξ, and t. x characterizes the momentum fraction of the struck quark in the quark loop and, as such, is not directly accessible experimentally except in the measurement of the beam spin asymmetry. ξ is the longitudinal momentum fraction of the transfer Δ, with $\xi = x_B/(2-x_B)$ in the Bjorken limit. $t = \Delta^2$ is the standard momentum transfer between the virtual and real photons.

H and E are spin-independent, and $\tilde{H}$ and $\tilde{E}$ are spin-dependent functions. More precisely, the light-cone matrix element of the bilocal quark operator that enters in these hard-electroproduction reactions (represented by the lower blobs in Fig. 1) is at leading twist in Q^2 given by:

$$\begin{aligned}
&\frac{P^+}{2\pi}\int dy^- e^{ixP^+y^-}\langle p'|\bar{\Psi}_\beta(-\frac{y}{2})\Psi_\alpha(\frac{y}{2})|p\rangle\Big|_{y^+=\vec{y}_\perp=0} \\
&= \frac{1}{4}\Big\{(\gamma^-)_{\alpha\beta}\left[H^q(x,\xi,t)\;\bar{N}(p')\gamma^+N(p)\;+\;E^q(x,\xi,t)\;\bar{N}(p')i\sigma^{+\kappa}\frac{\Delta_\kappa}{2M_N}N(p)\right] \\
&\quad +(\gamma_5\gamma^-)_{\alpha\beta}\left[\tilde{H}^q(x,\xi,t)\;\bar{N}(p')\gamma^+\gamma_5N(p)\;+\;\tilde{E}^q(x,\xi,t)\;\bar{N}(p')\gamma_5\frac{\Delta^+}{2M_N}N(p)\right]\Big\} \quad (1)
\end{aligned}$$

with $P = (p + p')/2$ and q a quark flavor index. This formula explicitly shows the vector (axial) nature of the H, E ($\tilde{H}$, $\tilde{E}$) GPDs associated or not associated with the γ_5 matrix.

The H and $\tilde{H}$ are generalizations of the parton distributions measured in deep inelastic scattering. In the forward direction (defined by $\Delta = 0$), H reduces to the quark distribution $q(x)$, and $\tilde{H}$ to the quark-helicity distribution $\Delta q(x)$ measured in deep inelastic scattering. Furthermore, at finite momentum transfer, there are model-independent sum rules that relate the first moments of these GPDs to the standard hadronic form factors.

$$\begin{aligned} \int_{-1}^{1} H^q(x,\xi,t)dx &= F_1^q(t), \\ \int_{-1}^{1} E^q(x,\xi,t)dx &= F_2^q(t), \\ \int_{-1}^{1} \tilde{H}^q(x,\xi,t)dx &= G_A^q(t), \\ \int_{-1}^{1} \tilde{E}^q(x,\xi,t)dx &= G_P^q(t), \quad \forall\xi \end{aligned} \tag{2}$$

Also, Ji [1] has shown that the second moment of these GPDs gives access to the contribution of the sum of the quark spin and the quark orbital angular momentum to the nucleon spin.

$$\frac{1}{2}\sum_q \int_{-1}^{1} \left(H(x,\xi,t=0) + E(x,\xi,t=0)\right) x dx = J_q \quad \forall\xi \tag{3}$$

A measurement of this sum rule would determine the contribution of the quark orbital angular momentum to the nucleon spin. However, we point out that this is not within the goals of the proposed experiment.

The GPDs reflect the structure of the nucleon independently of the reaction that probes the nucleon. They can also be accessed through the hard exclusive electroproduction of mesons, $\pi^{0,\pm}$, $\rho^{0,\pm}$, ω, ϕ,..., (see Fig. 1b) for which a QCD factorization proof was given recently [5]. It also showed that leading-order pQCD predicts that the vector meson channels ($\rho_L^{0,\pm}$, ω_L, ϕ_L) are sensitive only to the unpolarized GPDs (H and E), whereas the pseudoscalar channels ($\pi^{0,\pm}, \eta, ...$) are sensitive only to the polarized GPDs ($\tilde{H}$ and $\tilde{E}$). In contrast to meson electroproduction, DVCS depends on *both* the polarized and unpolarized GPDs.

Models of GPDs were obtained by direct calculations in the bag model [6], chiral soliton model [7], light-cone formalism [8], and also through a phenomenological construction [9, 10] based on the relation of GPDs to the usual parton densities.

Figure 2 shows the x and ξ dependence of $H(x,\xi,t=0)$ as an example of such a construction. The ξ dependence shows the changing character of the quark correlations from pure quark and antiquark distributions at $\xi = 0$, to strongly correlated

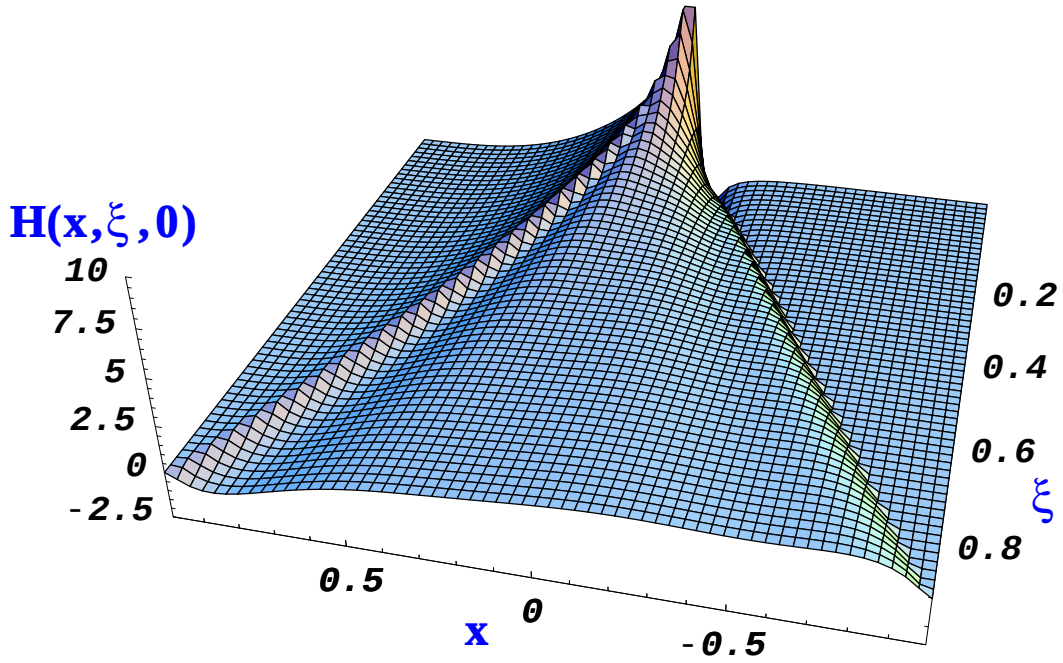

Figure 2: $H(x, \xi, 0)$ in the model of Ref. [10]

$q\bar{q}$ pairs at large values of ξ. The shape and magnitude the GPDs also depends on the momentum transfer t. This opens up another dimension in the study of GPDs. The t dependence is particularly sensitive to the transverse momentum distribution of the quarks.

2.2 Deeply Virtual Compton Scattering

DVCS is the most promising channel for studying GPDs at lower energies and Q^2. The dominance of the handbag diagram and the behavior of the reduced forward cross section as $1/Q^4$ (scaling regime) is expected to be reached at lower Q^2 than in the case of deep exclusive meson production. This is supported by measurements of the $\gamma^*\gamma\pi^0$ form-factor in e^-e^+ collisions. In leading-order pQCD, the DVCS process and the production of π^0 by two photons, where one of the photons is highly virtual, are described by the same kind of handbag diagram. Figure 3 shows recent measurements of $F_{\gamma^*\gamma\pi^0}$ from CLEO [11]. The curves correspond to leading order pQCD calculations [12] with next to leading order corrections. As is evident from the figure, $F_{\gamma^*\gamma\pi^0}$ starts to scale as $1/Q^2$ already at $Q^2 \sim 3$ GeV^2. The higher order corrections describe the data well for $Q^2 > 1$ GeV^2. This result strongly suggests that GPDs can be accessed through the study of DVCS at moderate Q^2.

The proposed experiment measures DVCS via the interference with the Bethe-Heitler (BH) process, Figure 4. The measured cross section of the reaction $ep \rightarrow ep\gamma$ is given by the sum of the DVCS and BH amplitudes, up to a phase space factor:

$$\frac{d^5\sigma}{dQ^2 dx_B dt d\phi} \propto |\mathcal{T}^{VCS} + \mathcal{T}^{BH}|^2 . \tag{4}$$

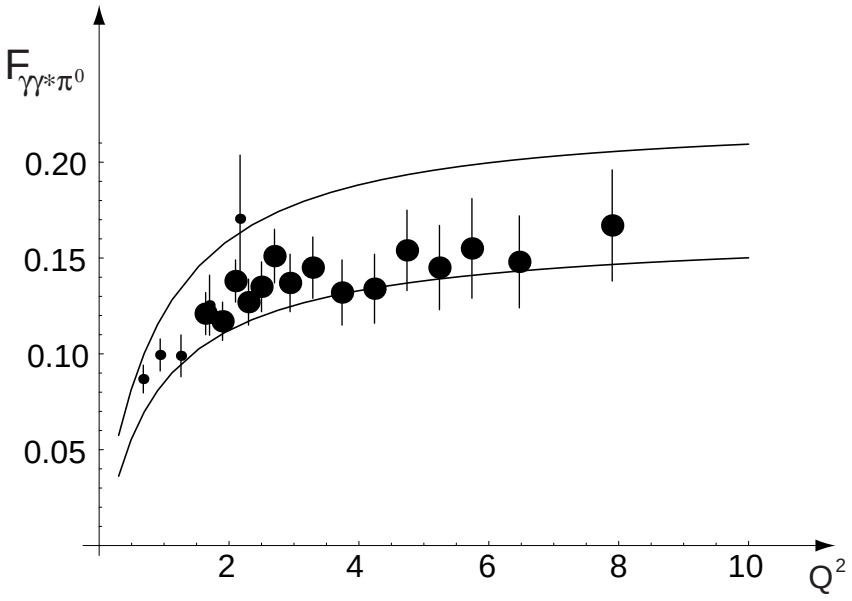

Figure 3: Experimental data on $Q^2 F_{\gamma^*\gamma\pi^0}$ from [11] with pQCD predictions using an asymptotic shape for the pion distribution amplitude (lower curve) and Chernyak-Zhitnitsky model (upper curve). The calculations include higher order corrections.

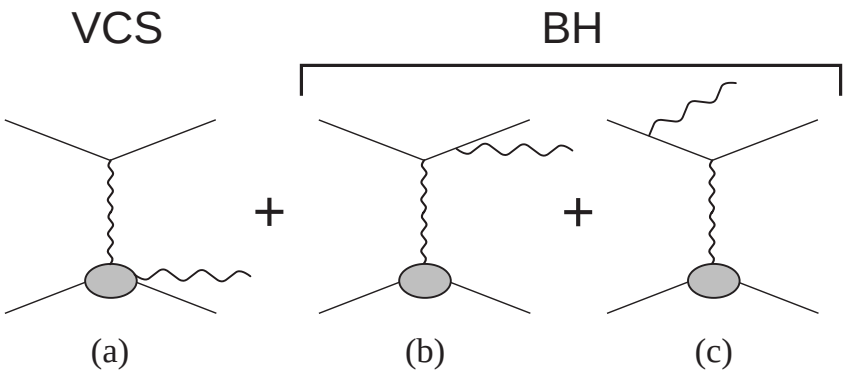

Figure 4: Feynman diagrams for VCS and Bethe-Heitler processes contributing to the amplitude of $ep \to ep\gamma$ scattering.

At beam energies accessible at Jefferson Lab, the BH contribution in the cross section is predicted to be several times larger than the DVCS contribution in most regions of phase space [10] (see Fig. 5).

The large BH process may be turned into an advantage by using a longitudinally polarized electron beam: one can measure the helicity-dependent interference terms that are proportional to the imaginary part of the DVCS amplitude. In this case the pure BH contribution is subtracted out in the cross section difference. The systematic errors then only apply to this difference. Expanding the BH amplitude in powers of $1/Q$, but keeping the complete helicity structure for the $\gamma^* p \to \gamma p$ process [14], the helicity-dependent cross section difference is of order $1/Q$ and given by

$$\frac{d^5\sigma^+}{dQ^2 dx_B dt d\phi} - \frac{d^5\sigma^-}{dQ^2 dx_B dt d\phi} \propto \mathrm{Im}(\mathcal{T}^{DVCS}) \times \mathcal{T}^{BH}$$
$$\propto \frac{1}{Q}\left[-\sqrt{\frac{1+\epsilon}{\epsilon}} \cdot \mathrm{Im}\tilde{M}^{1,1} \cdot \sin\phi + \mathrm{Im}\tilde{M}^{0,1} \cdot \sin 2\phi\right] + \mathcal{O}\left(\frac{1}{Q^2}\right) \quad (5)$$

where "+" and "-" denote positive and negative beam helicities. $\mathcal{T}^{DVCS}$ and $\mathcal{T}^{BH}$ are the amplitudes of the DVCS and BH processes, ϵ is the usual virtual photon polarization parameter, ϕ is the azimuthal angle between electron and hadron planes, and $\tilde{M}^{1,1}$ and $\tilde{M}^{0,1}$ are helicity amplitudes for transverse and longitudinal virtual photons, averaged over the proton helicity. In leading order, only $\tilde{M}^{1,1}$ contributes, and, therefore, the dominant $\sin\phi$ dependence should be observed.

The beam spin asymmetry is simply obtained from the ratio of the expressions (4) and (5):

$$BSA \equiv \frac{\sigma^+ - \sigma^-}{\sigma^+ + \sigma^-} = \frac{\sigma^+ - \sigma^-}{2\sigma} \quad (6)$$

The denominator is dominated by a ϕ independent BH term, but contains also, to lower order in $1/Q$, ϕ dependent terms with contributions both from pure BH and from the BH-DVCS interference. The latter may be expressed as a function of the real parts $\mathrm{Re}\tilde{M}^{\lambda,1}$ [14].

Figure 6 shows the predicted asymmetry evaluated at 5.75 GeV beam energy for $Q^2 = 2$ GeV^2, $-t = 0.3$ GeV^2, and $x_B = 0.3$ [13]. The asymmetry is large, about 0.4 to 0.45. The curves correspond to two models for the ξ-dependence of the GPDs.

An important aspect of the measurements of cross section differences for different helicities is that they probe GPDs at specific values of x, assuming the dominance of the handbag diagram: in this case, $\mathrm{Im}\tilde{M}^{1,1}$ is given by a sum of GPDs at $x = \pm\xi$. The same is true for the numerator of the beam spin asymmetry. This allows one to obtain more direct information on the x dependence of the GPDs. In contrast, in cross section measurements, GPDs appear in convolution integrals over x, through $\mathrm{Re}\tilde{M}^{1,1}$.

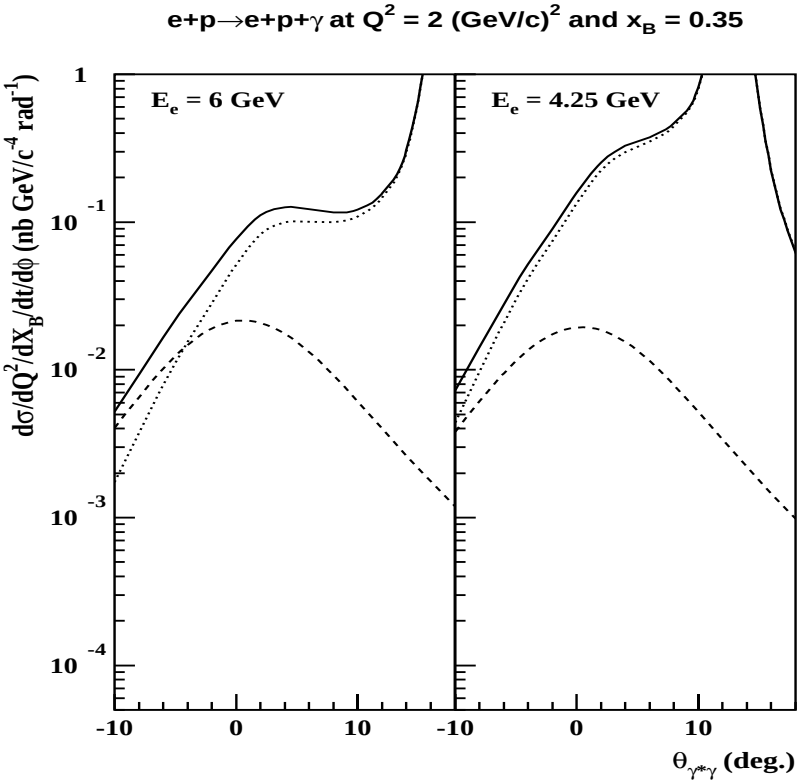

Figure 5: Cross section of $ep \rightarrow ep\gamma$ as a function of the angle between the virtual and real photons at beam energies of 4.25 (right), and 6 GeV (left), for $Q^2 = 2$ GeV^2 and $x_B = 0.35$. The positive values of $\theta_{\gamma\gamma^*}$ correspond to $\phi = 0$, and the negative to $\phi = 180°$. The dashed line is the contribution of DVCS, the dotted line represents the Bethe-Heitler part, and the solid line is the total sum (Eq. (4)). The cross sections are calculated according to Ref. [13].

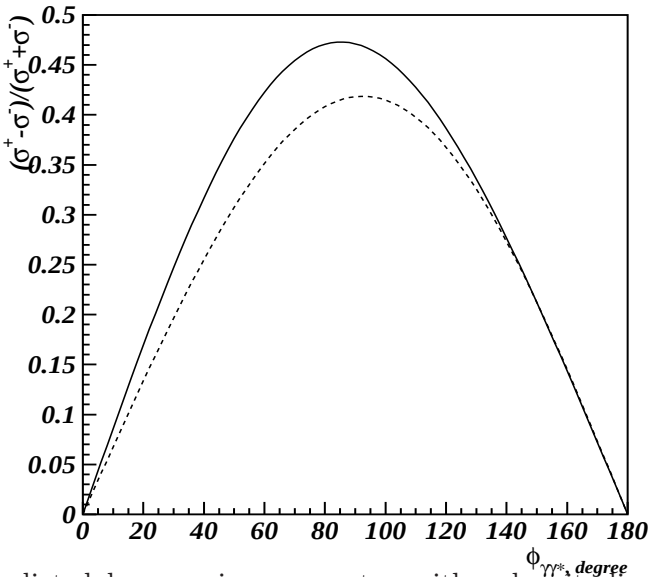

Figure 6: Predicted beam spin asymmetry with a longitudinally polarized 5.759 GeV electron beam. Kinematics are fixed at $Q^2 = 2$ GeV^2, $-t = 0.3$ GeV^2, and $x_B = 0.3$. The calculations from Ref. [13] are shown with (solid) and without (dashed) ξ-dependent parametrizations of the quark distribution functions.

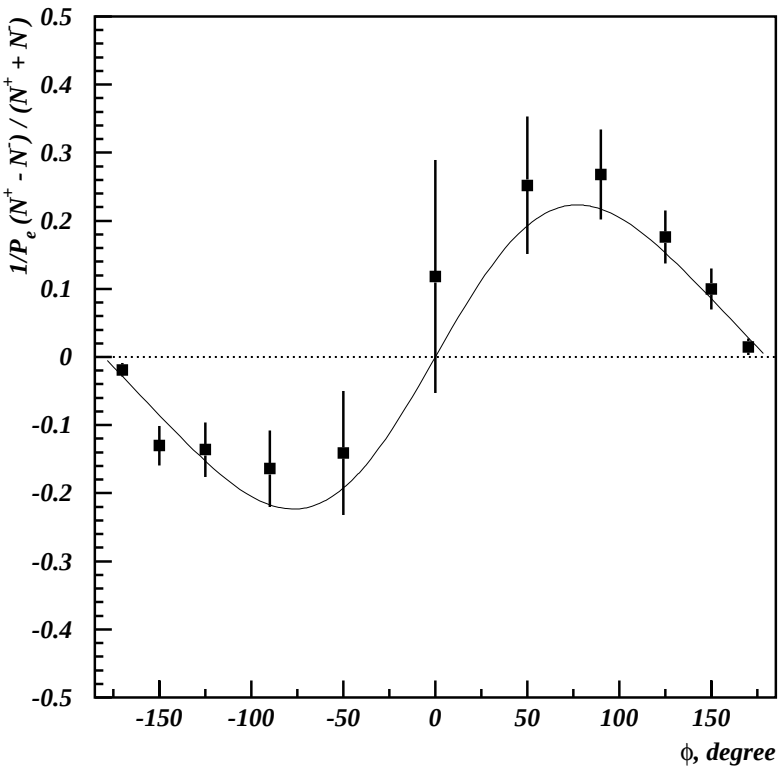

Figure 7: ϕ dependence of the $ep \rightarrow ep\gamma$ Beam Spin Asymmetry at 4.25 GeV. Data are integrated over the range of Q^2 from 1 to 2 GeV^2, x_B from 0.13 to 0.35 (with the condition $W > 2$ GeV) and $-t$ from 0.1 to 0.3 GeV^2. The curve is the fit to the function $A \sin\phi + B \sin 2\phi$.

3 Experimental situation

3.1 Recent evidence from JLab with CLAS

The DVCS/BH interference has recently been measured for the first time using CLAS. The data were collected as a by-product during the 1999 e1 run with a 4.25 GeV polarized electron beam. At energies above 4 GeV, the CLAS acceptance covers a wide range of kinematics in the deep inelastic scattering domain (W $\geq$ 2 GeV and $Q^2 \geq 1$ GeV^2). The open acceptance of CLAS and the use of a single electron trigger ensures event recording for all possible final states.

For the DVCS analysis, the reaction $\vec{e}p \rightarrow epX$ was studied and the number of single photon final states was extracted by fitting the missing mass (M_X^2 distributions. The beam spin asymmetry is calculated as:

$$BSA = \frac{1}{P_e} \frac{\left(N_\gamma^+ - N_\gamma^-\right)}{\left(N_\gamma^+ + N_\gamma^-\right)} \tag{7}$$

Here P_e is the beam polarization, $N_\gamma^{+(-)}$ is the extracted number of $ep \rightarrow ep\gamma$ events at positive (negative) beam helicity.

The resulting ϕ-dependence is shown in Fig. 7. A fit to the function

$$F(\phi) \;=\; A\sin\phi \;+\; B\sin 2\phi \tag{8}$$

yields $A = 0.217 \pm 0.031$ and $B = 0.027 \pm 0.022$. If the handbag diagram dominates, in the Bjorken regime, B should vanish and only the contribution from transverse photons should remain, described by parameter A.

3.2 JLab proposals

Two experimental proposals at the Jefferson Laboratory are approved for the study of exclusive reactions, with the initial aim to test whether the hard scattering regime may be reached at $Q^2 < 4$ GeV^2, and for x_B of the order of 0.35 (valence quarks).

3.2.1 Hall B - E99-105

Experiment 99-105 [15] is a major component of the E1-6 run scheduled with CLAS next fall. Its first goal is to measure the Q^2 dependence of the $ep \to ep\rho_L, (\omega_L, \phi_L)$ reactions, and to test the underlying s-channel helicity conservation (SCHC) hypothesis.

3.2.2 Hall A - E00-110

Experiment 00-110 [16] is not yet scheduled, but is aiming to run in Hall A in the second half of 2002. The DVCS beam spin asymmetries and cross section differences will be measured at three Q^2 intervals, for a fixed interval of x_B. The experiment will provide a precise check of the Q^2 dependence of the $ep \to ep\gamma$ cross section differences (for different beam helicities). Our proposal has an overlap with this experiment, but is directed toward a much larger kinematical coverage, extends to higher Q^2, and explores the x_B and t dependencies. A more detailed comparison with this experiment is presented in the Appendix.

3.3 Experiments at HERA

3.3.1 HERMES

From HERMES, preliminary beam polarization asymmetries have been shown [17]. These results suffer from the rather low luminosity. Moreover, the final state baryon is not unambiguously constrained to be a proton (Δ's and possibly other baryon resonances may contribute to the measured signal). It may be hard to extract from this measurement a truly exclusive DVCS signal. The HERMES collaboration has plans to implement a recoil proton detector to remedy the situation. Still, it is unlikely that high statistics can be achieved given the low luminosity of the HERMES operation.

3.3.2 H1 and ZEUS experiments

Photon events at high energy have been shown at conferences. However, the lack of exclusivity certainly affects the reported DVCS events at HERA [18]. Moreover, in this case, because of the very small values of x_B, it is in a good part the nucleon gluon content which is probed.

3.4 CERN experiment

A dedicated DVCS experiment at CERN is being studied for the COMPASS detector [19]; it is not expected to run before 2004. It would use the 200 GeV muon beam from the SPS and the COMPASS set-up augmented by a specially designed proton recoil detector. The high beam energy ensures that the DVCS process dominates over the Bethe-Heitler contribution. Cross section measurements are then possible, however beam asymmetries will not be accessible. The low luminosity limits the measurements to values of Q^2 only slightly higher than this proposal, and to smaller values of x_B (0.02 to 0.3).

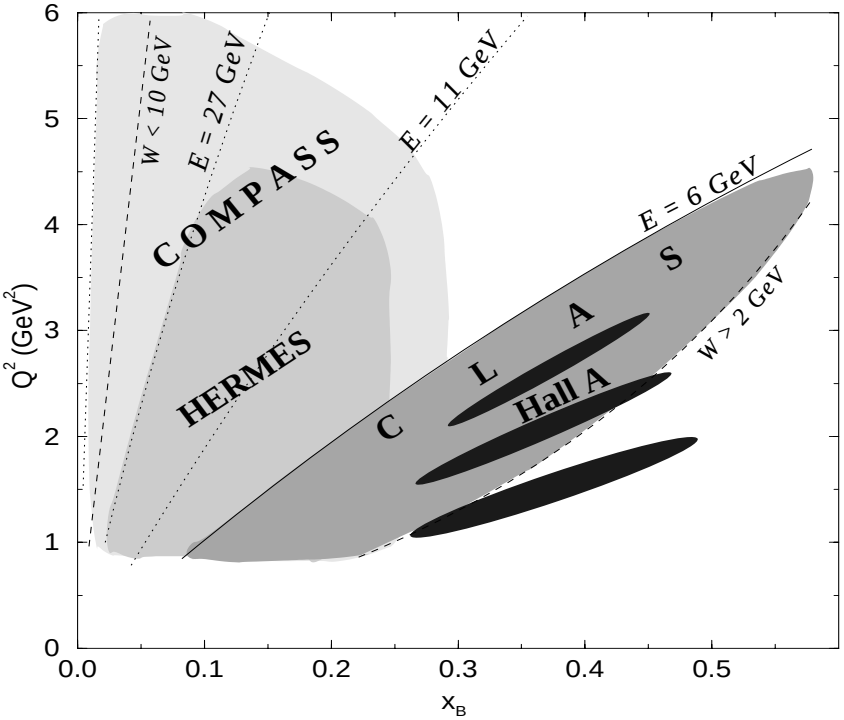

Figure 8: Kinematics coverage for various planned or proposed DVCS experiments.

Figure 8 illustrates the kinematical coverage of these experiments. It shows the broad interest at many laboratories to measure the DVCS process as a means of accessing the GPDs. In the short term, CEBAF with its 6 GeV beam can contribute uniquely to exploratory measurements of deep exclusive reactions, and of DVCS in particular.

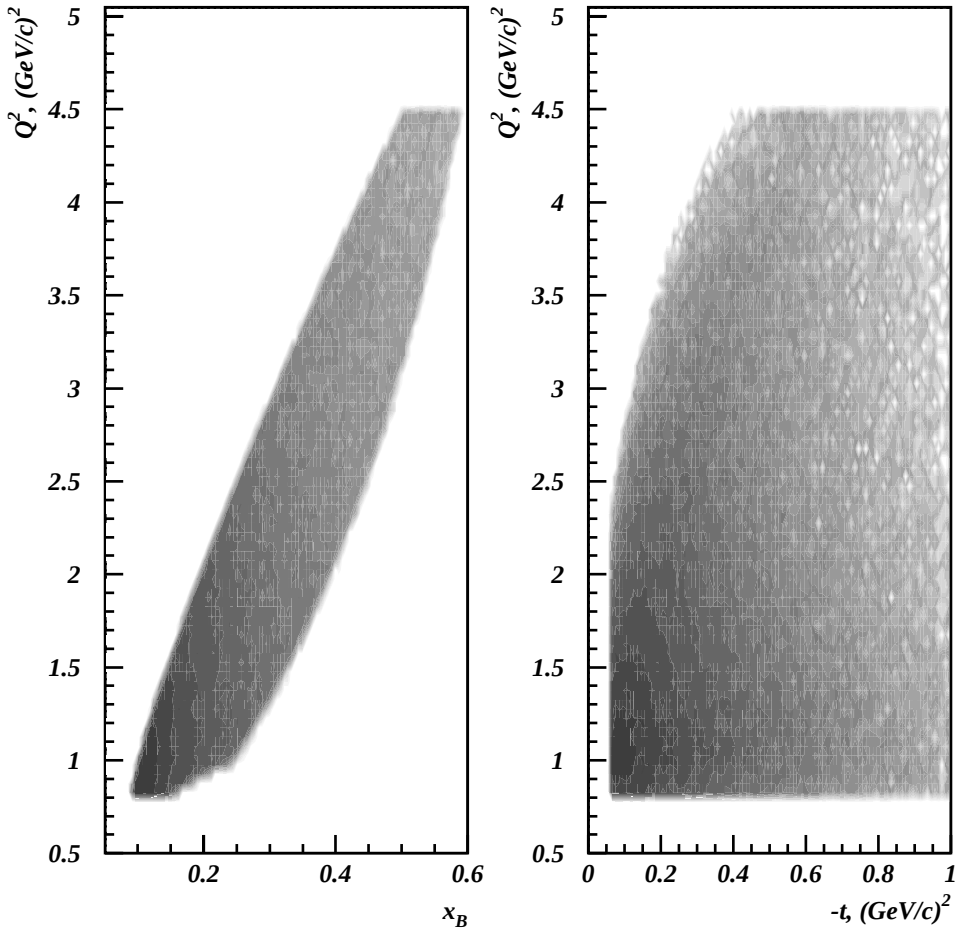

Figure 9: The accessible range of Q^2, x_B and t with CLAS at 6 GeV beam energy. Simulations are done for torus current $I_T = 3375$ A and for target position $Z_{trg} = -60$ cm.

4 A dedicated DVCS experiment in Hall B

The main goal of the proposed experiment is to measure the t and x_B dependence of the beam spin asymmetry for several fixed Q^2 bins (see Fig. 9). This quantity is sensitive to the model description of the GPDs. This will be the first time this dependence is studied using the DVCS process. A second goal will be to extract the helicity-dependent cross section difference, which directly determines the imaginary part of the DVCS amplitude.

Finally, the measurement of the $ep \rightarrow ep\gamma$ cross section will allow additional tests of the Q^2-dependence to check the scaling behavior. As CLAS covers a broad kinematic range, we will be able to test the Q^2 dependence of the DVCS process for different x_B. This will verify if we are in a regime where a direct interpretation of the results in terms of GPDs is possible. Possible observation of strong scaling violations would provide important input for the analysis in terms of higher twist QCD effects.

4.1 An optimized CLAS configuration

The nominal CLAS geometry has been designed for optimal use at beam energies up to 4 GeV. At higher energies some of the phase space of interest in exclusive reactions in the deep inelastic domain at high Q^2 and small momentum transfer t requires the

detection of particles at forward angles. For the nominal target position, and using the standard mini-torus as a magnetic shield for Møller electrons produced in the target, the minimum angle for the detection of charged particles, and high energy photons is approximately 10°. A significant portion of the photon yield is lost due to the acceptance limitations at small angles.

We plan on several changes to the nominal CLAS setup to optimize the conditions for the measurement of the DVCS process in two respects: firstly, to reach higher luminosities, and secondly, to increase the kinematic coverage for the direct detection of high-energy photons, both from the DVCS process, as well as from the decay of high momentum π^0.

The following changes to the standard CLAS configuration are needed:

1. Move the target position by about -60 cm upstream,
2. Optimize the lead shielding pipe,
3. Replace the mini-torus shield with a solenoidal magnetic field,
4. Install a lead tungstate $PbWO_4$ crystal array for the detection of high-energy photons to cover lab angles from 3 to 12 degrees.

Moving the target upstream is necessary to allow for the installation of a photon detector within the Region I drift chamber while maintaining sufficient angle resolution to separate single photons from $\pi^o \to \gamma\gamma$ events.

The first two modifications require only minor changes. A similar geometry was used during the EG1 experiments where a dynamically polarized ammonia target was installed in CLAS. Items 3 and 4 require more significant modifications in the setup of the inner CLAS detector system; however, minimal R&D work is needed since use of established techniques are proposed. The changes are outlined in the following sections. The proposed setup is shown in Fig. 10 and in a more detail in Fig. 11. A perspective view of the proposed photon detector is shown in Fig. 15.

4.1.1 A solenoidal shielding magnet for Møller electrons

The main source of background produced in an high-energy electron beam inpinging upon a hydrogen target is due to interactions of the electron beam with the atomic electrons (Møller scattering). This rate is several orders of magnitude larger than the inelastic hadronic production rate. In CLAS, this background is largely eliminated by the installation of the so-called mini-torus, a normal conducting toroidal magnet, designed to shield the Region I tracking chambers from the charged electromagnetic background. This allowed CLAS to reach the highest luminosities achieved in a large acceptance detector to date. The mini-torus introduces a cut-off in the minimum angle for particles (charged or neutrals) that can be detected in CLAS. This angle is about 10 degrees. For the proposed experiment the angle range below 10 degrees is

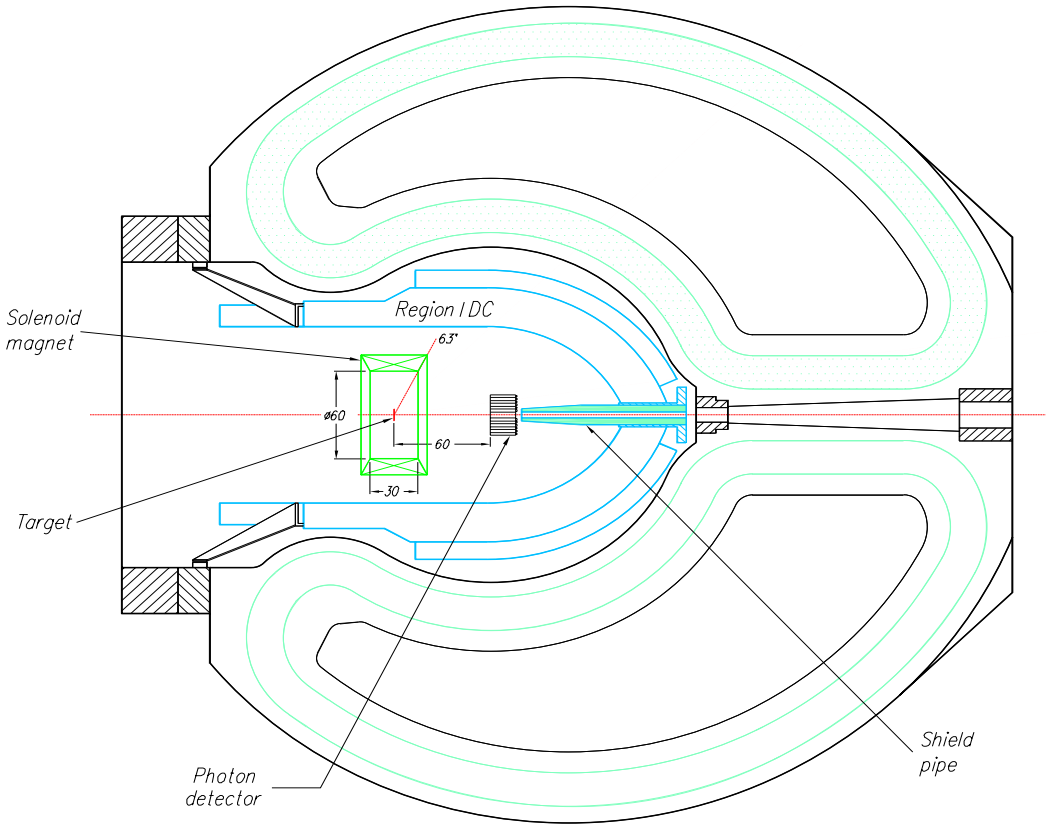

Figure 10: CLAS arrangement proposed for the dedicated DVCS measurement. The two straight red lines indicate the angle acceptance for photon detection in the CLAS forward electromagnetic calorimeter, showing that there is an overlap in acceptance between the EC and the $PbWO_4$ wall.

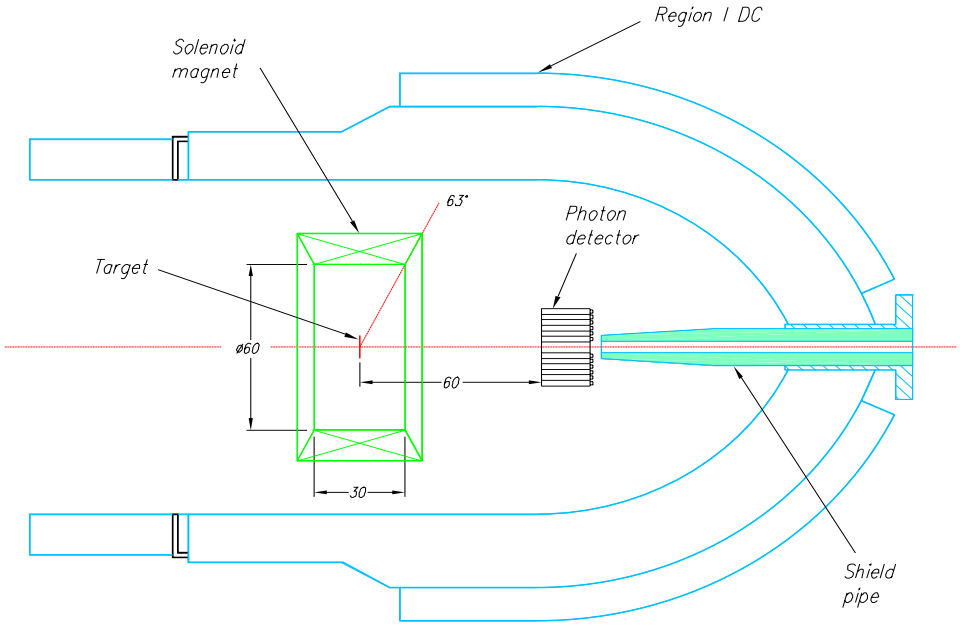

Figure 11: Inner detector layout for the proposed dedicated DVCS measurement

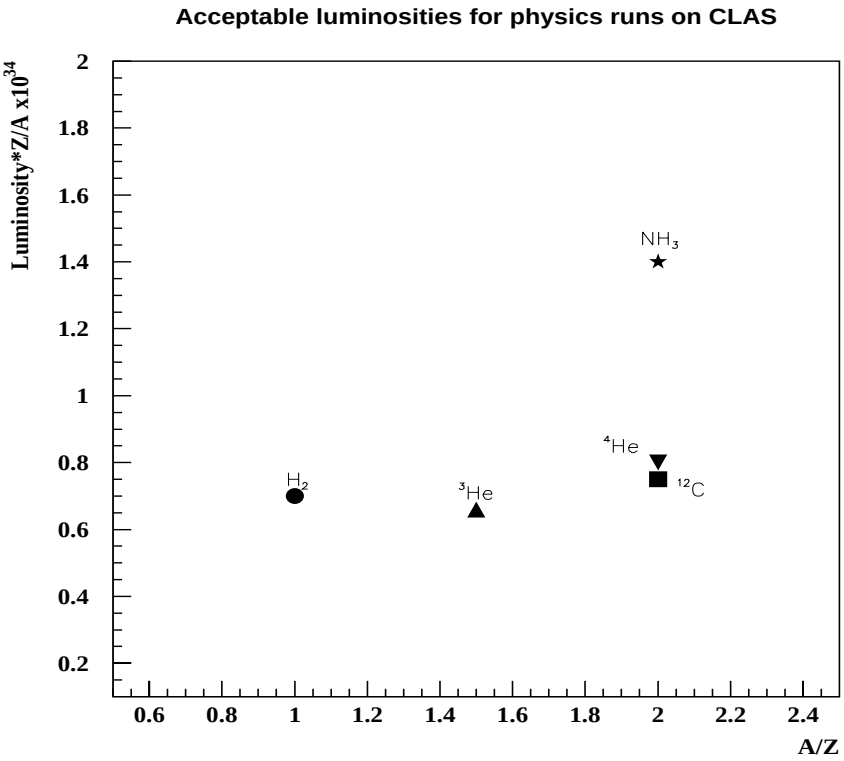

Figure 12: Maximum luminosities used during various electron scattering experiment. The points are multiplied by Z/A of the scattering target to obtain the hydrogen-equivalent luminosity. The point labelled NH_3 was obtained during operation with a longitudinal magnetic field during polarized target operation

important for the detection of high energy photons. An alternative to the standard mini-torus operation is therefore needed. A solenoidal magnet would not have these restrictions.

During the EG1 run periods the mini-torus was replaced by a superconducting Helmholtz configuration with a 5 T magnetic field at the target location oriented parallel to the electron beam. This magnet was designed with the goal of generating a homogenous magnetic field across the polarized target sample. At the same time, it reduced the Møller background seen in CLAS significantly. Tests during the EG1 experiment showed that the detector could tolerate higher luminosities than during operation with the mini-torus. This behavior had been expected from detailed simulations that were done prior to the installation of the polarized target magnet. Figure 12 shows the luminosity limitations during electron runs using different targets. The polarized target operation at 5.75 GeV (labeled NH_3 in Figure 12) shows approximately a factor of two increased luminosity in terms of a hydrogen-equivalent target material.

We propose to use a solenoidal magnetic field for shielding the CLAS detectors against charged electromagnetic background.

Detailed Monte Carlo simulations have been performed to optimize a solenoidal magnetic field configuration for use in the proposed experiment. The magnetic field distribution along the beam axis is shown in Fig. 13. Examples of simulated tracks from Møller electrons are shown in Fig. 14. We used a central solenoid field of 3 T and

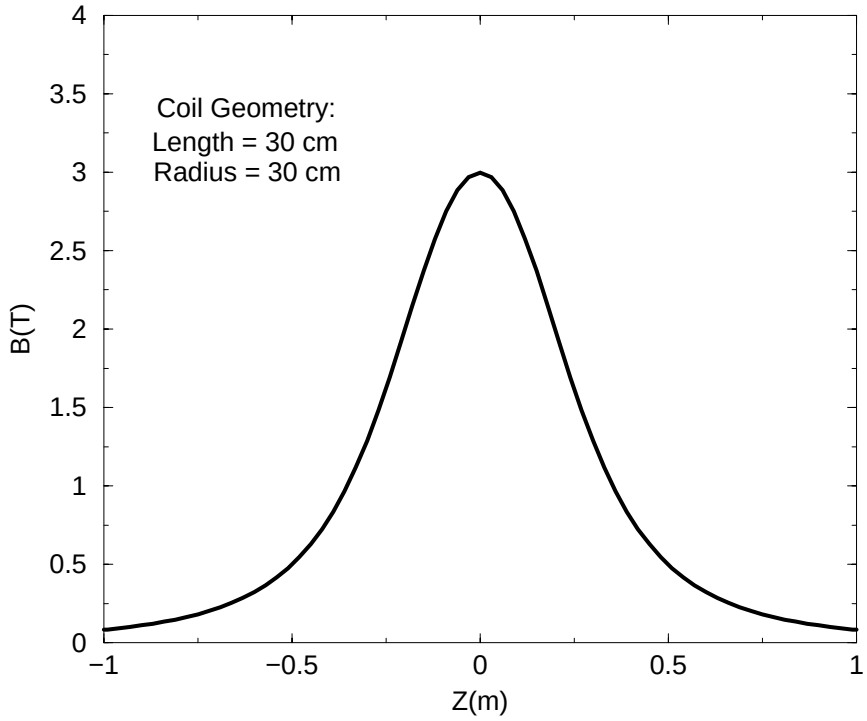

Figure 13: Magnetic field distribution along the beam axis generated by the proposed solenoidal shielding magnet. The target is located at the magnet center.

the target located in the center of the magnet. For these conditions the simulations show that the Møller electrons are confined in a cone with an opening angle of about 2.5° as seen from a 1 m distance to the production target. In order to minimize the size of the opening for the beam, the shape of the innermost crystals will be modified to obtain a circular opening of about 2.5 degrees in the midplane of the array (not shown in the figure). Also, the maximum field strength of the magnet should be 4 - 5 Tesla to provide sufficient flexibility for the positioning of the target and the photon detector.

Møller electrons, which are the vastly dominating source of electromagnetic background, will pass through the central penetration in the lead-tungstate wall, and be absorbed in the downstream shielding pipe. The shielding arrangement is very similar to the one used during the EG1 run which absorbed practically all of the Møller electrons.

From our experience with the Helmholtz shielding magnet during the EG1 run period we expect at least a factor of two higher luminosity than during previous E1 runs. The Helmholtz magnet used in EG1 was, however, not optimized as a magnetic shield but to generate a homogeneous magnetic field across the target volume. With a solenoid magnet, which is taylored to optimize the shielding performance, we expect to reach luminosities of about 2×10^{34} cm^{-2}s^{-1}, or about a factor of 3 higher than during previous E1 run periods.

We expect that the solenoid magnet will be superconducting. However, we do not

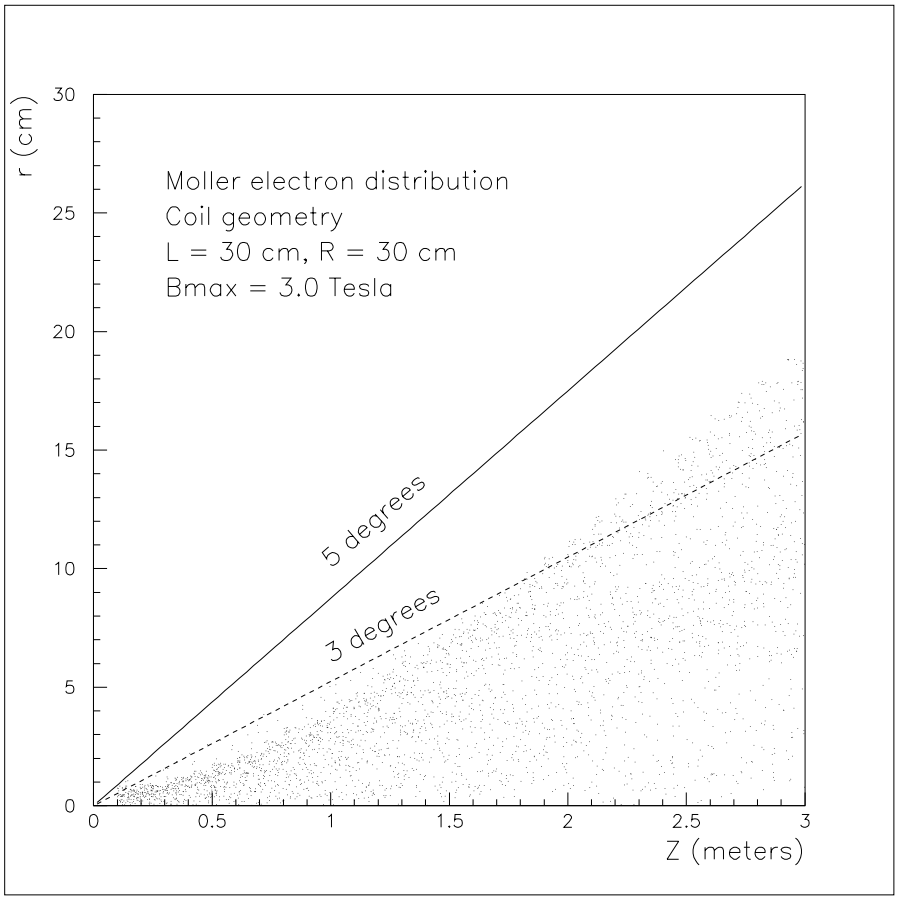

Figure 14: Simulation of Møller electron motion in the solenoidal magnetic field.

expect any significant problem in the design or construction of such a magnet. The already mentioned superconducting Helmholtz magnet used during the EG1 experiment had much more stringent requirements as far as field homogeneity and precision of the coil geometry are concerned, while the maximum field was 5 T, and the total $\int Bdl$ are both approximately 2 Tm. In order to allow use of the CLAS liquid hydrogen target inside the solenoidal field volume, and also to allow particles to enter the CLAS tracking regions at angles up to 60 degrees, the solenoid magnet must have a warm bore for free access to the target area. This is not the case for the existing Helmholtz magnet.

4.1.2 A photon detector for small angle coverage

From our analysis of the 4.25 GeV data, we conclude that the biggest contribution to the systematic uncertainty in the DVCS/BH asymmetry resulted from the separation of single photon events from π^o events, and from other background contributions. Since the π^0 yield could not be measured directly, for lack of adequate photon detection, this contribution could not be subtracted. The resulting systematic uncertainty of $\approx 10\%$ in the asymmetry was still adequate since the statistical error was significantly larger.

The situation can be significantly improved if the photons are detected directly.

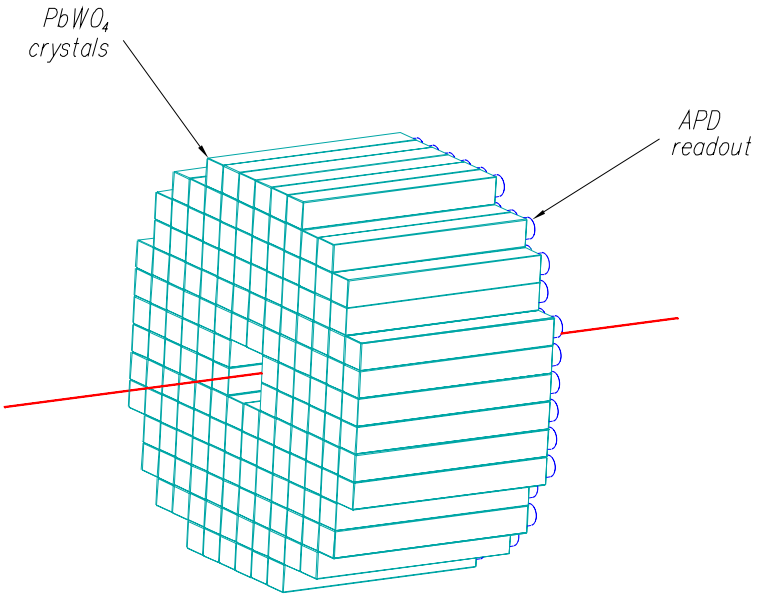

Figure 15: A view of the proposed $PbWO_4$ crystal wall.

Even after taking into account the new target position, the minimum detection angle for the existing CLAS electromagnetic calorimeter is about 8°. Morever, its acceptance is much reduced at small scattering angles due to the CLAS torus coils. Therefore, even at the highest Q^2 and x_B, less than 50% of the direct photons can be measured, while at the lowest Q^2 photons cannot be detected in the standard CLAS configuration.

The situation can be significantly improved with the implementation of a forward angle photon detector covering the angle range from about 3 degrees to 12 degrees. The required small dimensions of the detector call for a high density material. A $PbWO_4$ crystal array emerged as a leading candidate for such a detector. The array[3] consists of 160 crystals with 20 mm by 20 mm cross section, and a length of 160 mm (18 radiation lengths). The lateral size was chosen to roughly correspond to the Molière radius of 22 mm. This guarantees good position resolution due to the lateral spread of shower energy to adjacent crystals.

The array is positioned at a distance of 60 cm downstream from the target position (Fig. 11). The innermost 4 crystals are removed for the beam to pass through. The array is positioned in front of the shield pipe to allow detection of photons down to angles of about 3 degrees. The high density of the lead-tungstate crystals (radiation

[3]For the purpose of this proposal, we only discuss $PbWO_4$ as material, and avalanche photo diode for light readout. However, we are also considering other options such as lead-fluoride crystals, and photomultipliers for light readout.

length $L_o = 8.9$ mm) is crucial for containing the entire shower in a small array.

Our collaborators from ITEP in Moscow have assembled a 5 by 5 crystal array. Extensive tests were carried out in a test beam, showing excellent performance of the crystals. To read out the light produced in the crystals, avalanche photodiodes (APD) are used. Although they have a much smaller gain compared to regular photomultipliers, they have the important advantage of being insensitive to the strong magnetic field at the crystal location. The use of low noise preamplifiers allows detection of minimum ionizing particles. A $\sigma_{noise} = 7$ MeV noise contribution was achieved in these tests, while minimum ionizing particles will deposit about 150 MeV of energy. The energy loss of minimum ionizing particles can thus be used as a means of energy calibration, and monitoring. For high energy photons the energy resolution is not affected by the noise contribution.

Energy resolution

In the simulations we used conservative estimates for all contributions to the energy resolution. Assuming that 9 channels will be summed up to determine the photon energy, the energy resolution is parametrized as:

$$\frac{\sigma}{E} = \frac{0.05}{\sqrt{E(\mathrm{GeV})}} + 0.005 + \frac{0.05}{E(\mathrm{GeV})} \quad .$$

The first two terms are based on test results from the LHC CMS detector, the third contribution is based on our own tests of APDs , where we have doubled the noise contribution obtained in laboratory tests. The resulting energy resolution is then expected to be comparable to or somewhat better than the one for the CLAS EC. However, significant improvements in APD technologies have occured since the CMS tests were carried out leading to significantly reduced noise contributions if low noise preamplifiers are used. These advances will be employed in the proposed experiment.

Further improvements in the energy resolution could be obtained if magnetic field insensitive photomultipliers were used. This option is still being studied.

Position resolution

Position resolution of similarly shaped $PbWO_4$ crystals have been measured for the CMS detector at CERN [20]. They can be parametrized as:

$$\frac{\sigma_r}{E} \approx \frac{2.6 \text{ mm}}{\sqrt{E}} \; + \; 0.3 \text{ mm} \quad ,$$

where we have increased the first term by 10% to account for the slightly larger lateral crystal dimensions proposed for this experiment. At the planned position, 60

cm downstream from the production target, this corresponds to an angle resolution of approximately 5 mr at 1 GeV, which is the minimum energy for the photons of interest.

Stability of response

Lead-tungstate crystals are known to be rather sensitive in their light output to temperature changes. The ambient temperature therefore has to be stabilized, or at least monitored, and the crystal/APD response carefully monitored. While we are still weighing the various options, we plan on monitoring the stability of the crystal responses using a laser driven fiber optics calibration system. A controlled amount of light is injected into the crystals via quartz fibers and the response recorded and used to monitor the gain.

Two $PbWO_4$ crystals are currently being tested in CLAS. They are located in an area of high magnetic field to simulate conditions similar to the conditions of the proposed setup.

4.1.3 Trigger and data acquisition

We are planning to use the standard trigger, data acquisition, and online monitoring system of CLAS. The signal amplitude and time information will be read out using standard Fastbus ADC and TDC boards currently in use in CLAS. The crystal array information will be read out for every event, but not used in the trigger. An additional 160 channels of ADCs and TDCs will be needed. We plan to use the standard CLAS level 1 trigger to select scattered electrons, and the level 2 to select one additional charged particle. No changes to the trigger hardware are anticipated.

4.1.4 Calibration

The crystal array will be calibrated in-situ using minimum ionizing particles selected from the reaction $ep \rightarrow ep\pi^+(\pi^-)$ where the π^- kinematics are inferred from 4-momentum vector conservation. This technique is used routinely in calibrating the CLAS tracking efficiency. Other reactions, such as $ep \rightarrow ep\pi^0$, can be used to calibrate the EC and $PbWO_4$ wall with photons.

4.2 Event identification, reconstruction, acceptances

Event identification in CLAS is accomplished using charged particle tracking in the toroidal magnetic field, time-of-flight, and momentum information. Electrons are separated from heavier particles using threshold gas Cherenkov detectors, and electromagnetic calorimeters.

Electron and proton momenta are reconstructed in the CLAS driftchamber system using the standard CLAS software. For the proposed dedicated experiment, photons from direct production and from π^0 decays (or from η decays) will be reconstructed using the new small angle photon detector and the CLAS forward angle EC. This will provide large acceptance coverage for both reactions.

The reaction $ep \rightarrow ep\gamma$ can, in principle, be identified through the determination of the missing mass M_X in the reactions $(ep\gamma X)$ and (epX). This method was used successfully in the analysis of the 4.25 GeV data, and we want to use the same method for the 5.75 GeV E1-6 run. However, the missing mass resolution achieved in CLAS is not good enough to have a separation of the $ep\gamma$ and $ep\pi^0$ final states event by event. We therefore used a technique that analyses the line shape of the missing mass distribution to separate the two contributions. The systematic error estimated for the resulting DVCS/BH asymmetry is considerably larger compared to the direct detection of photons. However, for the 5.75 GeV E1-6 run the resulting statistical errors are comparable to the expected systematic uncertainties of this method.

For the dedicated run at 6 GeV, and with much higher statistics, detection of photons in the CLAS EC and the new small angle photon detector is mandatory and will allow separation of single photons from π^0's event by event. We estimate that single photons can be separated from π^0's for momenta up to 4 GeV/c by direct reconstruction. Rejections of π^0's from a shower profile analysis will work to considerable higher momenta, although this is not required for this experiment.

4.2.1 Separation of single γ from $\gamma\gamma$ events.

Accidental coincidences do not play any significant role in electron scattering experiments with CLAS because of the low luminosity and the good time resolution. The main sources of background to the $ep\gamma$ final state will be from $ep\pi^0$ and from $ep\gamma\gamma$ events, where only one of the two photons is detected. The former process will be measured directly for the same kinematics as the $ep\gamma$ process, and can be subtracted. The latter reaction corresponds to hadronic production of two photons, which can be measured in the experiment, or inelastic radiative corrections. The latter ones are dominated by processes when the incoming electron radiates off a photon (which escapes detection in the beam pipe) and e.g. N^* resonances are excited, which subsequently decay into a proton and a photon. The electromagnetic decay is suppressed by typically two orders of magnitude in comparison to a hadronic process, and the invariant mass of the $\gamma\gamma$ final states results in a broad range in the epX missing mass. Most of these events will be eliminated by missing mass cuts. However, the usual radiative corrections are needed to determine the unradiated cross section.

To be more definite, we simulated the following processes: $ep \rightarrow ep\gamma$, $ep \rightarrow ep\pi^0$, $ep \rightarrow ep\gamma\gamma$, where we assumed a $1/Q^4$, and e^{-4t} behavior for the Q^2 and t dependences of the cross sections, respectively. The ϕ-modulation was simulated according to the CLAS DVCS data at 4.2 GeV. The final state $ep\gamma\gamma$ was generated

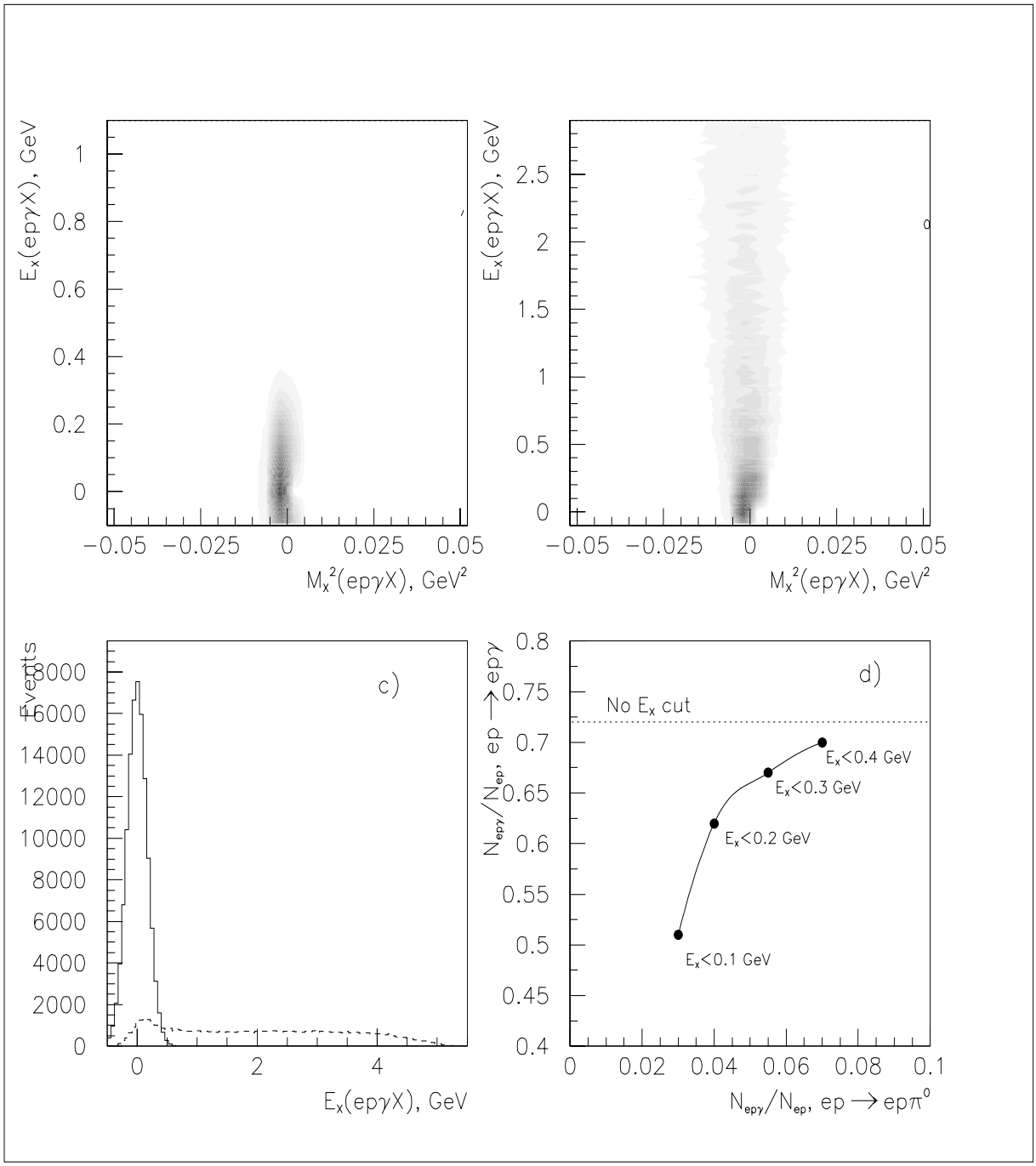

Figure 16: Separation of $ep\gamma$ and $ep\gamma(\gamma)$ events using the missing mass and missing energy method. The top panels show the missing energy from $ep\gamma$ (left) and $ep\pi^0$ (right) events if only one photon is detected versus missing mass for $ep\gamma X$. The projection of both graphs is shown at the bottom left. The π^0 contamination is a small fraction under the single photon peak. The bottom right panel shows the probability for a π^0 to be misidentified as a single photon on the horizontal axis and the single photon detection probability on the vertical axis a function of the missing energy cut.

Table 1: Accepted/generated $ep\gamma$ events - from various processes

E_X(GeV)	$ep\gamma$ $N_{ep\gamma}/N_{ep}$	$ep\pi^0$ $N_{ep\gamma}/N_{ep}$	$ep\gamma\gamma$ (direct) $N_{ep\gamma}/N_{ep}$	$ep\gamma\gamma$ (radiative) $N_{ep\gamma}/N_{ep}$
0.2	0.65	0.04	0.06	0.005
0.4	0.7	0.07	0.1	0.01

according to a double emission of photons, randomly distributed according to the same t-dependence, and according to the radiative process with subsequent excitation and decay of excited states. The detection probability for both photons from the π^0, the direct $ep\gamma\gamma$, and radiative $ep\gamma\gamma$, is 0.55, 0.50, and 0, respectively. The latter reaction (inelastic radiative correction), which can not be measured directly, has a small detection probability for the non-radiative photon (see last column in the Table 4.2.1). It is the main part of the inelastic radiative corrections.

The use of a combination of the epX and $ep\gamma X$ missing masses allow isolation of single photon as well as π^0 events. This is described in Fig. 16. It shows the efficiency for the detection of single photons, and the probability for the rejection of π^0 events. The results are summarized in table 1:

In table 1 E_X is the cut on the missing energy as in panel a) and b) of Fig. 16. Complete kinematical fits will further improve this separation. For example, one can also make use of the required co-planarity for the direct $\gamma^*\gamma p$ events, while $\gamma^*\gamma p$ from $ep\pi^0$ events will generally not be co-planar.

In kinematical areas where the π^0 yield is much smaller than the photon yield, for example in the angle range below 3 degrees, which is not covered by calorimetry, the missing mass method may still be an effective way of measuring the beam spin asymmetry, although we are not counting on using this part of the phase space.

Figure 17 shows the acceptances for the detection of ep and $ep\gamma$ events integrated over the entire electron acceptance for the kinematics of interest.

4.3 Count rates and statistical errors

The expected number of counts is given by

$$N = \mathcal{L} \times \text{time} \times \sigma \times (\Delta Q^2 \cdot \Delta x_B) \times \Delta t \times \Delta\phi \times (\Delta\varphi_e)_{\text{eff}}/2\pi \qquad (9)$$

With the optimized configuration as described in Sec. 4.1, a luminosity of 2×10^{34} $\text{cm}^{-2}\text{s}^{-1}$ is expected. For 60 days of beam time, this corresponds to an integrated luminosity $\mathcal{L} \times \text{time} = 10^8$ nb^{-1}.

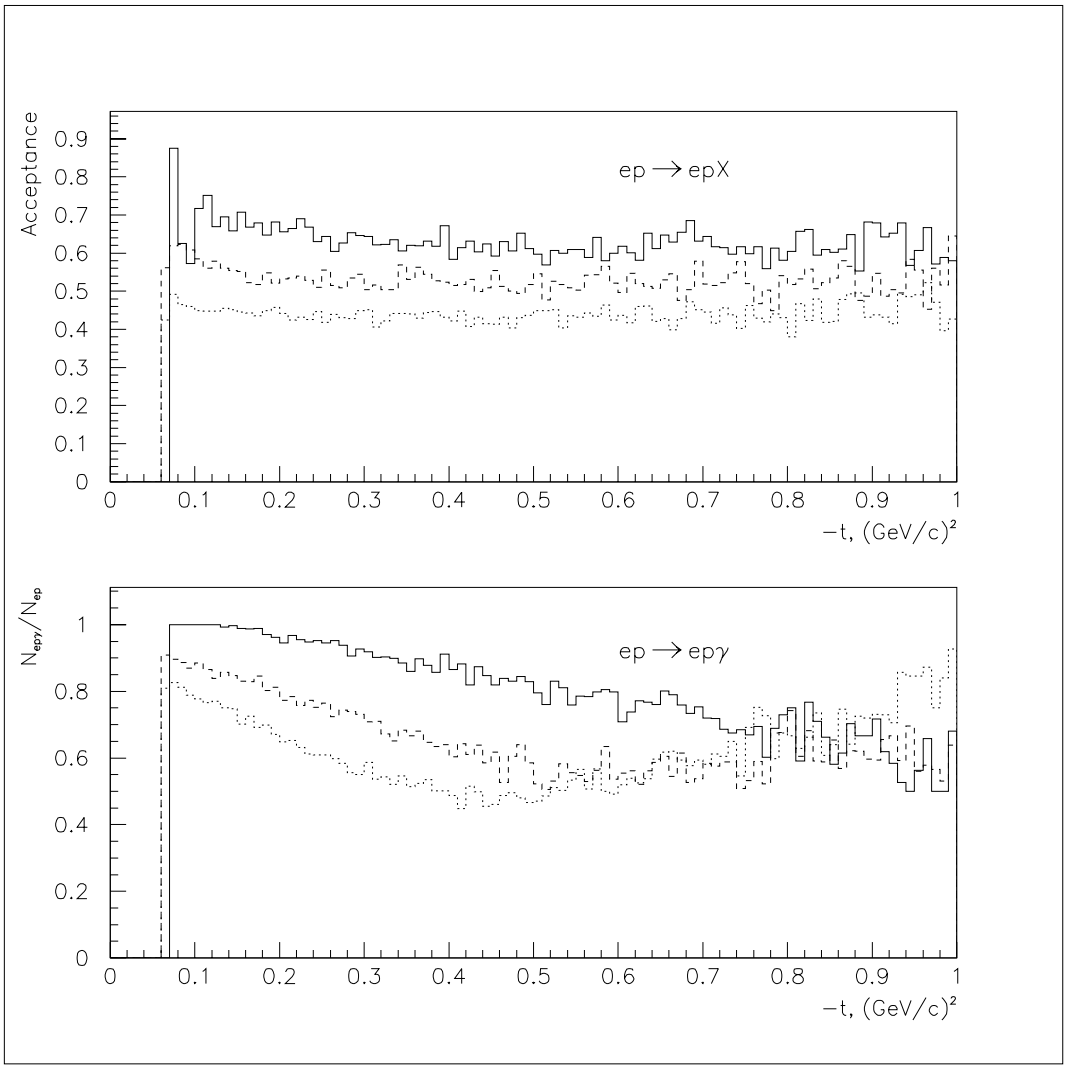

Figure 17: CLAS acceptances for $ep(\gamma)/e(p\gamma)$ (top) and for $(ep\gamma)/ep(\gamma)$ (bottom) final states in the reaction $ep \rightarrow ep\gamma$ at beam energy 6.0 GeV. The particle in () is not observed. CLAS torus current is 3375 A, target position 60 cm upstream from nominal CLAS center. $Q^2 = 1.5$ GeV^2 - dotted line; $Q^2 = 2.0$ GeV^2 - dashed line; $Q^2 = 3.0$ GeV^2 - solid line.

The cross sections are calculated following Refs. [10, 13], using the ξ-dependent parameterization of the GPDs. These calculations are valid to leading order for the handbag diagram and include the interference with the Bethe-Heitler process.

In a large acceptance detector like CLAS, the binning of the data according to the relevant kinematical variables is somewhat arbitrary. For the sake of presentation in a table and in figures, we have chosen here rather wide bins. It is very likely that the final data set will be subdivided into finer bins, for a better study of the Q^2, x_B and t dependences of the observables.

- The Q^2 and x_B bins are indicated in Table 2. The resulting area ($\Delta Q^2 \cdot \Delta x_B$) is smaller than the product $\Delta Q^2 \times \Delta x_B$ because of limitations in the electron scattering angle and of the requirement $W > 2$ GeV (see Fig. 9).

- The t range will be divided into three or four bins, taking into account the increasing value of $|t_{min}|$ at large (Q^2, x_B). The binning in $|t|$ will be the

Table 2: Indicative binning of data in Q^2 and x_B, together with the cross sections at the center of each bin and for $t = -.325$ GeV^2, $\phi = 90°$. The resulting number of counts are calculated according to Eq. 9, with $\Delta t = 0.15$ GeV^2 and $\Delta\phi = 30°$. See text for more explanations.

Q^2 (GeV^2)	x_B	σ (nb/GeV^4)	$\Delta Q^2 \cdot \Delta x_B$ (GeV^2)	$(\Delta\varphi_e)_{\rm eff}/2\pi$	N
$0.8 - 1.2$	$0.09 - 0.17$	0.45	0.03	0.34	38000
$0.8 - 1.2$	$0.17 - 0.27$	0.23	0.02	0.31	11000
$1.2 - 1.7$	$0.13 - 0.23$	0.18	0.04	0.40	23000
$1.2 - 1.7$	$0.23 - 0.35$	0.077	0.04	0.36	9000
$1.7 - 2.3$	$0.18 - 0.28$	0.10	0.05	0.46	18000
$1.7 - 2.3$	$0.28 - 0.42$	0.035	0.06	0.42	7200
$2.3 - 3.1$	$0.25 - 0.35$	0.056	0.05	0.54	12000
$2.3 - 3.1$	$0.35 - 0.50$	0.018	0.08	0.50	5800
$3.1 - 4.1$	$0.35 - 0.55$	0.015	0.12	0.64	9300

following: $(0.1 - 0.25)$, $(0.25 - 0.40)$, $(0.40 - 0.60)$ and $(0.60 - 0.80)$.

- The whole ϕ range will be divided into 12 bins of 30°.

This procedure would result into a total of 396 bins for the whole data set.

For the acceptance $(\Delta\varphi_e)_{\rm eff}/2\pi$, we used averaged values (over ϕ and t). The corresponding numbers in Table 2 are good to 10-15%, at the present stage of definition of this new set-up.

The resulting numbers of counts in Table 2 may appear large, but we reiterate that they correspond to bins much wider than desirable for our study. Also the cross sections at $\phi = 180°$are significantly smaller (see Fig. 20). These numbers are used to calculate the statistical uncertainties illustrated in the figures of the following section. A beam polarization of 0.75 is assumed for the calculation of $\Delta(BSA)$.

4.4 Systematic errors

The proposed spin asymmetry measurement is rather insensitive to systematic uncertainties such as acceptances and charge normalization. A significant contribution is expected from the beam polarization which is measured using Möller scattering with an accuracy of 0.010. Another contribution is due to possible contamination of the

single photon sample with misidentified photons from π^0 events. As these events will have a different asymmetry from single photon events they add an systematic error to the asymmetry. With the additional photon detector we will have excellent separation of $p\gamma$ and $p(\pi^0 \to \gamma\gamma)$ events. The π^0 asymmetry will be measured simultaneously and can thus be corrected for, as the size of the π^0 contamination can be measured as well. From the analysis of the 4.25 GeV data we conclude that the $ep(\pi^0)$ yield is generally smaller than the $ep(\gamma)$ yield except for some extreme kinematics where it may be comparable or larger.

We conservatively estimate the total systematic error of the asymmetry to ≈ 0.010. Since the peak asymmetry is expected to be 0.35, this will result in a 3% relative systematic error, sufficiently small for a very significant measurement.

Note that for the E1-6 portion of the proposal, we expect a systematic error about 2-3 times larger.

The secondary goal of the experiment will be a measurement of the absolute cross section differences for the DVCS process. CLAS was designed to measure absolute cross sections at the 3% level. Currently, accuracies of 2-5% have been achieved in the measurement of elastic ep cross sections. Another process that can be used for absolute normalization is $ep \to ep\pi^0$ at the peak of the $\Delta(1232)$ resonance. The cross section is known with an accuracy of better than 3%. Measurement of this reaction requires detection of the scattered electron and the outgoing proton. Measurements with CLAS show agreement with fits to the world data at the level of better than 5%. In addition to the epX cross section uncertainty we estimate a 3% uncertainty in the photon detection efficiency.

We add all systematic errors in quadrature we obtain a conservative estimate of 6.5% total systematic uncertainty for the $ep \to ep\gamma$ cross section.

When extracting the helicity-dependent cross section difference, the uncertainty in the beam polarization measurement, which we estimate at $\delta P_e \approx 0.01 - 0.015$, has to be taken into account as well.

4.5 Projected results and comparison to models

The following three graphs show some expected variations of the observables and a selection of expected data points.

Figure 18 shows the t dependence of the cross section and of the beam spin asymmetry, for three bins in Q^2 and x_B. Expected data points are shown only for $Q^2 = 2$ GeV^2 and $x_B = 0.35$, assuming a finer binning in t (compared to the discussion in Sec. 4.3): $\Delta t = 0.06$ GeV^2.

Figure 19 illustrates the x_B dependence, for various other fixed parameters. In this case, a finer binning in x_B was assumed: $\Delta x_B = 0.04$.

Finally, Fig. 20 shows the ϕ dependence, and the expected data points are shown with the original binning of Sec. 4.3.

Comparison with different models for the ξ-dependency of GPDs are included, together with a first estimation of the twist-3 effects for this process.

5 Data taking during the E1-6 run

For the first stage of the experiment we propose to take data concurrently with the e1-6 run group which is scheduled to run in the fall of 2001. A major part of the e1-6 run group is the study of GPDs in vector meson production at high W, high Q^2 and small t. This corresponds to kinematics similar to the ones we propose to study in this experiment.

The e1-6 run group is approved for 30 days of running at the highest available beam energy, which is currently 5.75 GeV. The proposed experiment will be the first DVCS experiment to run at high luminosity and the highest beam energy available at JLab. This will produce high quality data on the exclusive production of photons in the DVCS kinematics, and will be the first experiment with sufficiently high Q^2 to likely approach the scaling regime. On the other hand, the statistical accuracy will be sufficient only in the lowest Q^2 bins to test model predictions for the GPDs. We estimate that the total accumulated $ep(\gamma)$ events will be approximately a factor ≈ 6 smaller than in the proposed dedicated run. If the detection of the full $ep\gamma$ final state is required, this factor is > 12, and will depend on the target position which is currently not defined.

For this part of the data taking we will use the standard CLAS equipment with the mini-torus inserted in CLAS, and photon detection only in the forward CLAS electromagnetic calorimeters. Most of the analysis will therefore rely on the missing mass techniques used at lower energies. The kinematical coverage will be nearly the same as for the dedicated experiment, slightly reduced due to the somewhat lower energy. However, the statistical errors will be 2.5 times larger, and the systematic errors are estimated to be 2 - 3 times larger for the beam spin asymmetry measurement. Nevertheless, the 30 days of running will produce significant results for the beam spin asymmetry for the lower Q^2 bins.

6 Summary and beam time request

In this experiment we propose a study of the Generalized Parton Distributions (GPD) via measurements of Deeply Virtual Compton Scattering above the resonance region, and for $Q^2 > 1\text{GeV}^2$, using a 6 GeV electron beam and the CLAS detector. The first measurement will be carried out concurrently with the E1-6 run group using the existing CLAS configuration. The E1-6 group is scheduled to run for 30 days of beam time in the fall of 2001. The dedicated DVCS experiment, which is the main part of this proposal, will use CLAS in a modified configuration augmented by a solenoidal

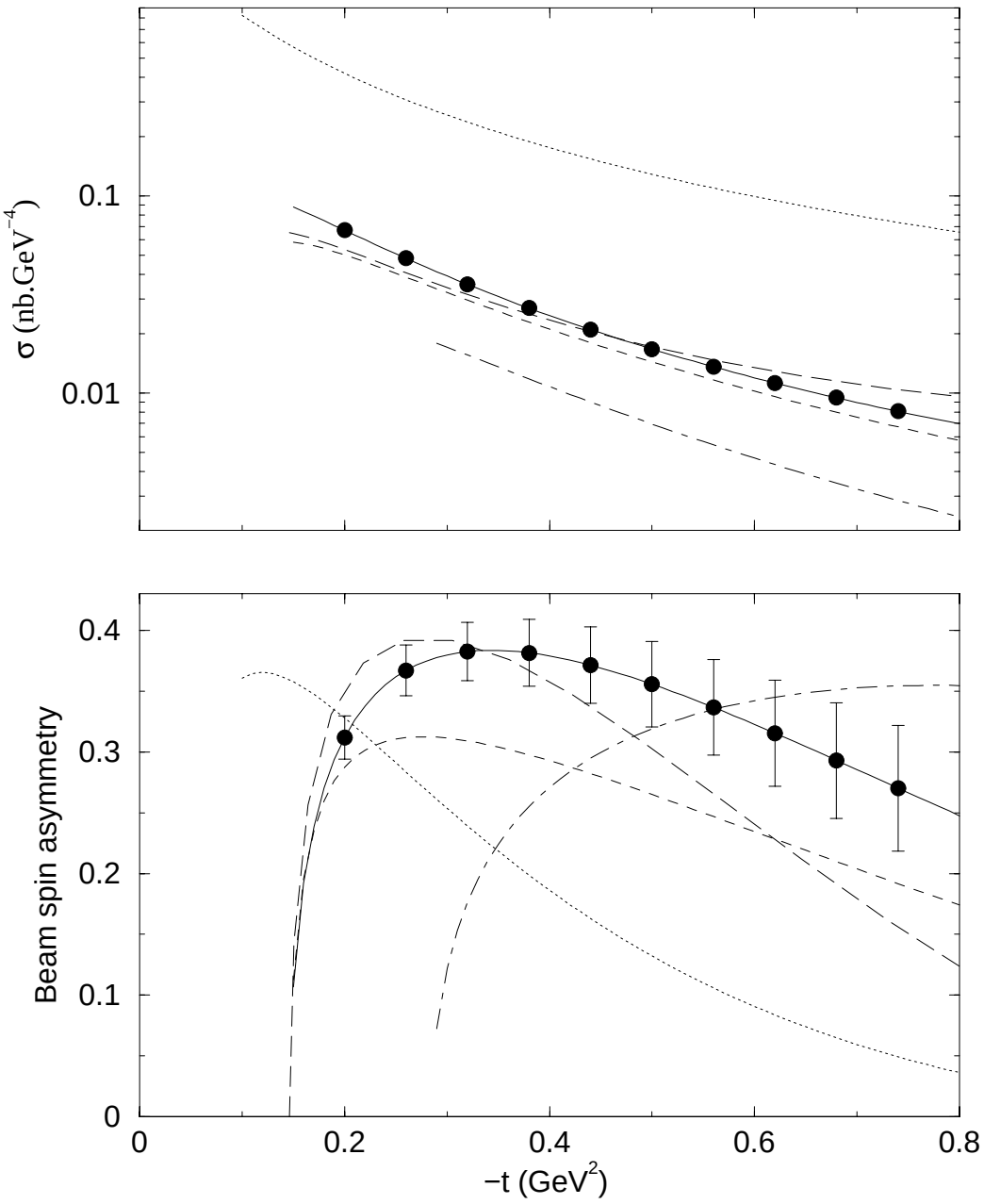

Figure 18: t-dependence of $ep \rightarrow ep\gamma$ observables at 6 GeV, for $\phi = 90^\circ$ and $Q^2 = 1$ GeV^2, $x_B = .22$ (dotted curve), $Q^2 = 2$ GeV^2, $x_B = .35$ (solid), $Q^2 = 3.6$ GeV^2, $x_B = .45$ (dot-dashed), calculated with the ξ-dependent GPDs of Refs. [10, 13]. From the same references is also shown the ξ-independent version (dashed), and from Ref. [21] the calculation including twist-3 effects (long-dashed), both at $Q^2 = 2$ GeV^2. Note that checks are in progress concerning (very) small inconsistencies between two different codes used to generate these curves. The points illustrate the expected statistical accuracy, for the bin sizes indicated in Sec. 4.3, except for $\Delta t = 0.06$ GeV^2.

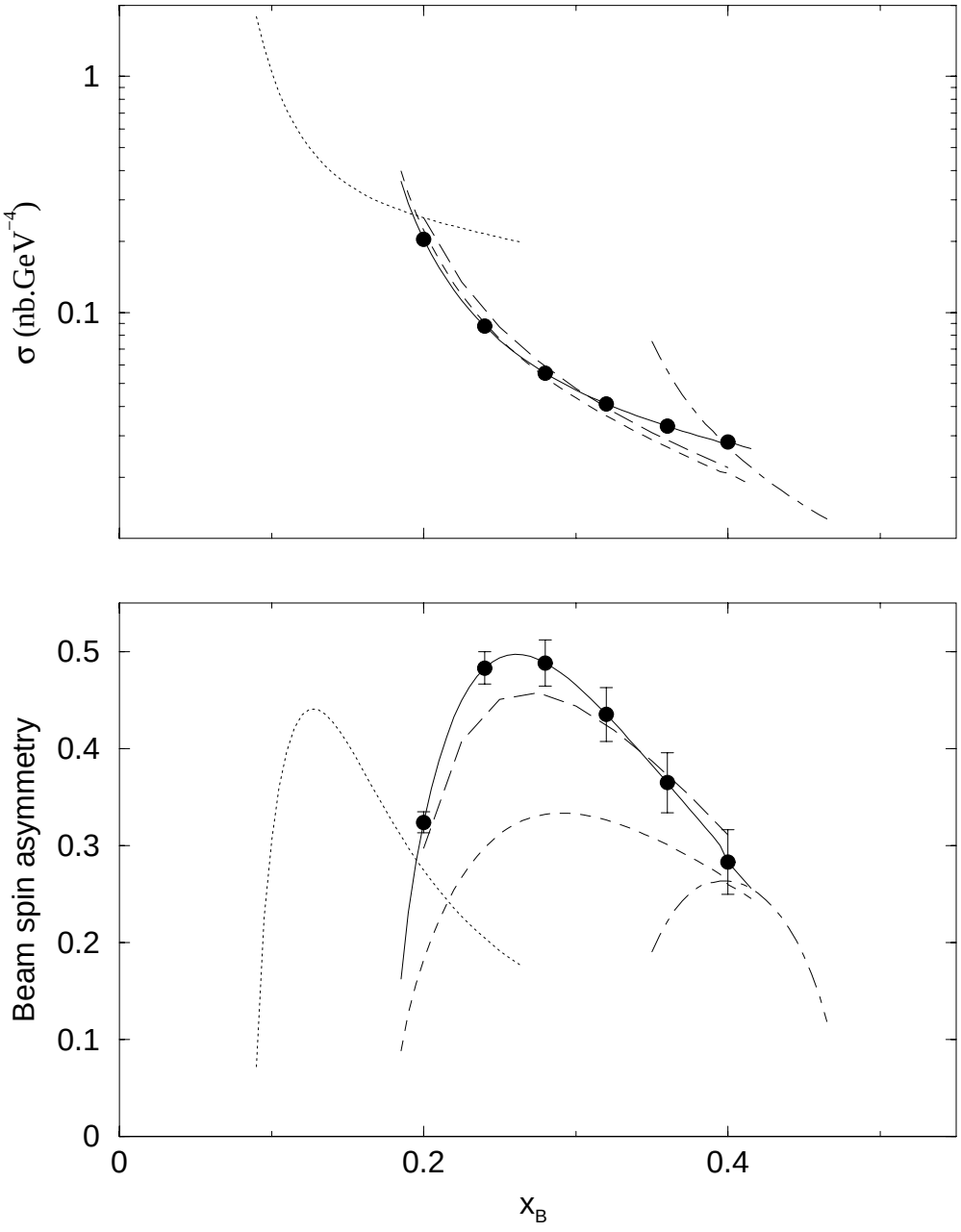

Figure 19: x_B-dependence of $ep \rightarrow ep\gamma$ observables at 6 GeV, for $\phi = 90°$, $t = -0.325$ GeV^2 and $Q^2 = 1$ GeV^2 (dotted curve), $Q^2 = 2$ GeV^2 (solid, dashed, long-dashed), $Q^2 = 3.6$ GeV^2 (dot-dashed). See Fig. 18 for remainder of the legend. The points illustrate the expected statistical accuracy, for the bin sizes indicated in Sec. 4.3, except for $\Delta x_B = 0.04$.

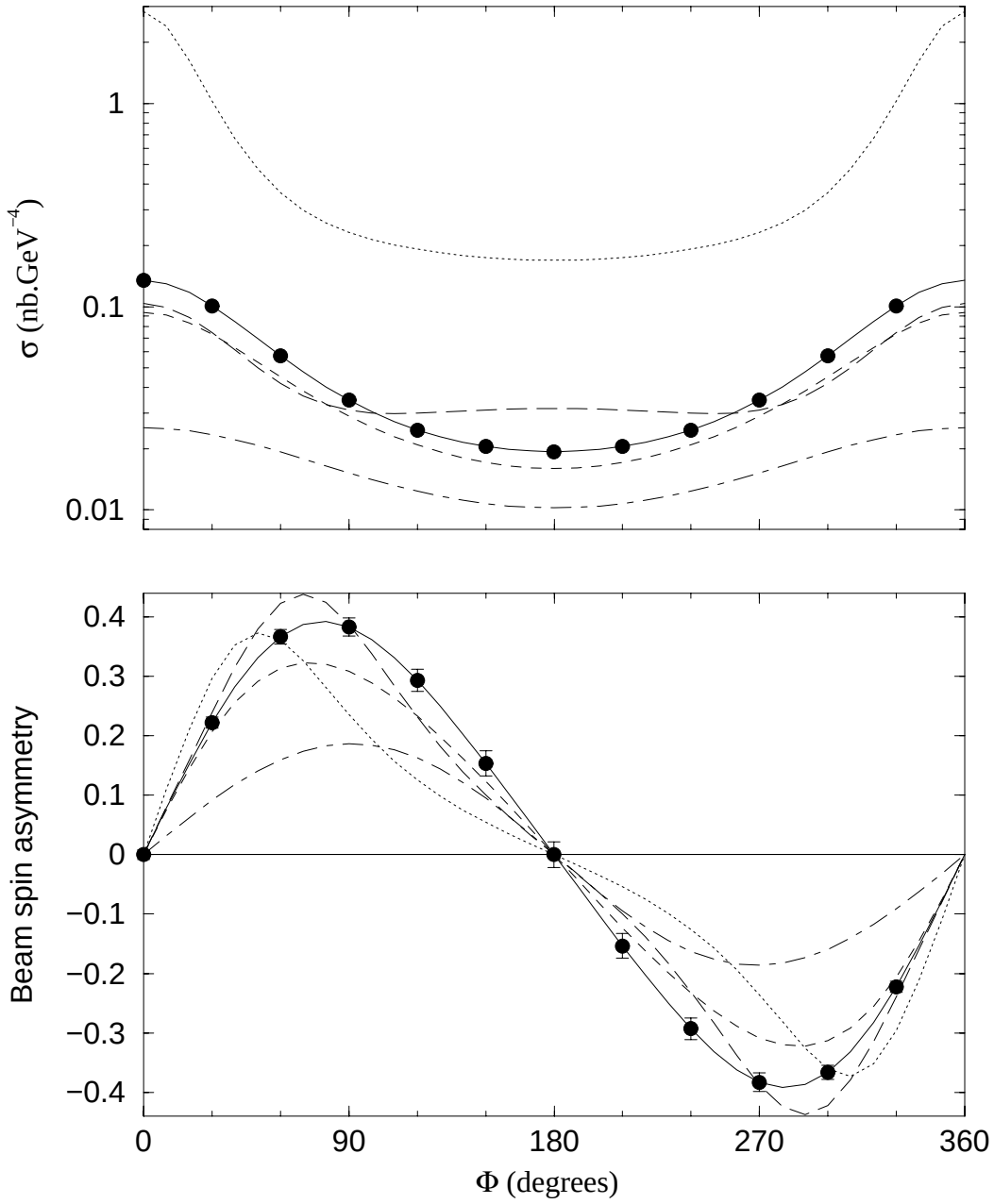

Figure 20: in Sec:4.3 ϕ-dependence of $ep \rightarrow ep\gamma$ observables at 6 GeV, for $t = -0.325$ GeV^2. The points illustrate the expected statistical accuracy at $Q^2 = 2$ GeV^2, for the bin sizes indicated in Sec. 4.3. See Fig. 18 for remainder of the legend.

shielding magnet and a small angle photon detector. For this proposal, we request new beam time of 60 days with highly polarized electrons at 6 GeV to access the maximum Q^2 range where the formalism of the GPD's is most likely to apply, but where cross sections are particularly low. We expect smaller systematic uncertainties than for the E1-6 run, due to the increased capabilities for the direct detection of high energy photons at small angles.

The DVCS process will be determined via interference with the Bethe-Heitler process by measuring the beam spin asymmetry. This asymmetry is directly comparable to calculations and predictions in terms of magnitude, Q^2, x_B and t behaviors.

We believe that the measurements that we intend to carry out in this proposal are an indispensable prerequisite for the development of the GPD field. It should also be clear that this kind of study involves a simultaneous scan of various variables (x_B, Q^2, t) and that a large acceptance detector such as CLAS is most suitable. Analyses of already existing electroproduction data from CLAS and studies based on simulations have shown that the proposed measurements are feasible.

In particular, current physics analyses show that we can measure absolute cross section in CLAS with an accuracy of $2\% - 5\%$. We conclude that allow us to measure absolute cross section differences in addition to the primary goal of determining beam spin asymmetries. The following table summarizes the relative merits of the two run periods.

Table 3: Beam requests and summary of relative merits for the two run periods

Proposal	$\mathcal{L}$ $cm^{-2}sec^{-1}$	$\int \mathcal{L}dt$ cm^{-2}	relative acceptance	beam time scheduled *days*	beam time new *days*	FOM *relative*
E1-6	7×10^{33}	1.7×10^{40}	1	30	—	1
dedicated run	20×10^{33}	10×10^{40}	> 2	—	60	12

The much improved figure-of-merit (FOM) for the dedicated measurement reflects the improvement in luminosity (a factor 3), acceptance for photon detection (>2, variable with kinematics), and longer running time (2). This will allow us to extend the kinematic range to higher Q^2 and to map out the x_B and t dependence in smaller bins.

Beam Request

We ask the PAC for an approval of the concurrent running for 30 days with the E1-6 run group, and to award 60 days of new beam time for a dedicated high statistics DVCS experiment.

The time needed to build our new equipment and get this experiment ready is estimated between 14 and 18 months.

Together with the expected Hall A results, the proposed DVCS measurement with CLAS will produce precision data on the imaginary part of the DVCS amplitude that will provide stringent tests of models for GPDs, which will unlikely be superseded by any of the currently planned DVCS experiments. Precise data for the DVCS process at 6 GeV, produced in a timely fashion, will also help maintain the momentum in the theory community. The focus here is on higher order corrections which likely will be important for a complete understanding of the expected results from the proposed measurement. We finally want to point out that the study of DVCS and Deeply Virtual Meson Production has been proposed as a major program for the 12 GeV energy upgrade of CEBAF.

Appendix: further comparison with Hall A experiment

Experiment 00-110 [16], aiming to run in Hall A in the second semester of 2002, is the first DVCS proposal in the laboratory. Following Sec. 3.2.2, we present here a more detailed comparison between our proposed DVCS measurement in Hall B and this conditionally approved Hall A experiment.

The Hall A experiment will provide a precise check of the Q^2 dependence of the $ep \to ep\gamma$ cross section differences (for different beam helicities). Systematic errors in the cross section normalization will be smaller in Hall A (2-3%) than in Hall B (6-7%). As for the beam spin asymmetry, it has already been shown, with both simulated and real data, that the CLAS acceptance introduces but small corrections in this observable (see Sec. 4.4).

The anticipated bin width will be larger in Hall B than Hall A (especially in $\Delta Q^2 \cdot \Delta x_B$). It should be noted however that the Hall A experiment integrates over a similar range of Q^2 and x_B, but with a high degree of correlation between these variables: the ellipses in Fig. 8 are the kinematical images of the High Resolution Spectrometer acceptance in the scattered electrons angles and energies. For a theoretical interpretation, one then needs to average the calculated observables over a similar kinematical range.

A quantitative comparison between this proposal and experiment E00-110 is given in Table 4. For Hall A, $\Delta\varphi_e$ is given by the HRS vertical acceptance (and but a small mismatch with the proton detector), while for Hall B it takes into account the correlated electron, proton and photon azimuthal acceptance. The indicated bin size for this proposal (in some sense arbitrary - see Sec. 4.3) results in similar count rates per bin as for the Hall A proposal. In the two regions of overlap, the statistical uncertainties would then be only slightly smaller for the Hall A experiment. The larger kinematical coverage for Hall B, in all four variables Q^2, x_B, t and ϕ, results in a significantly larger number of roughly equivalent bins (372 compared to 48).

Finally, the CLAS acceptance allows measurements around $\phi = 180°$, while the proton detector in the Hall A experiment does not cover this kinematical region. Yet, at 6 GeV and for not too large values of $|t|$, this is the only region where the magnitude of the DVCS amplitude becomes similar to, or even greater than, the one of the BH amplitude (see Fig. 5). This will provide first significant measurements of $\sigma - \sigma^{BH}$, as envisaged at JLab with an 11 GeV beam and at COMPASS.

Table 4: Quantitative comparison of Hall A E00-110 experiment and this proposal in Hall B. See text for discussion.

	Hall A	Hall B
$\mathcal{L}$ ($\mathrm{cm}^{-2}\mathrm{s}^{-1}$)	10^{37}	2×10^{34}
Number of days	20	60
Integrated luminosity (nb^{-1})	1.7×10^{10}	10^{8}
$(\Delta\varphi_e)_{\mathrm{eff.}}/2\pi$	0.025	~ 0.5
$\Delta Q^2 \cdot \Delta x_B$ (GeV^2)	0.015 - 0.030	0.03 - 0.12
Δt (GeV^2)	0.15 - 0.30	0.15 - 0.20
$\Delta\phi$	15°	30°
Luminosity $\times$ phase space (in $\mathrm{nb}^{-1}\cdot\mathrm{GeV}^4$, for average bin)	$\sim 5 - 6 \times 10^5$	$\sim 3 - 4 \times 10^5$
Number of settings	3	1
Number of bins per setting	16	396

References

[1] X. Ji, Phys. Rev. Lett. **78**, 610 (1997); Phys. Rev. D **55**, 7114 (1997).

[2] A.V. Radyushkin, Phys. Lett. B **380**, 417 (1996); Phys. Rev. D **56**, 5524 (1997).

[3] S. Stepanyan V.D. Burkert, L. Elouadrhiri et al. in preparation for Phys. Rev. Lett.

[4] D. Müller *et al.*, Fortschr. Phys. **42** (1994) 2,101.

[5] J.C. Collins, L. Frankfurt, and M. Strikman, Phys. Rev. D **56**, 2982 (1997).

[6] X. Ji, W. Melnitchouk and X. Song *Phys. Rev.* D **56**, 5511 (1997).

[7] V.Yu. Petrov et al., *Phys. Rev.* D **57**, 4325 (1998).

[8] M. Diehl, T. Feldmann, R. Jakob and P. Kroll, *Eur. Phys. J.* C **8**, 409 (1999).

[9] A.V. Radyushkin, Phys. Lett. B 449 (1999) 81.

[10] M. Vanderhaeghen, P.A.M. Guichon and M. Guidal, Phys. Rev. **D60**, 094017 (1999).

[11] J. Gronberg et al. (CLEO Collaboration), Phys.Rev. **D 57**, 33 (1998)

[12] I. V. Musatov and A. V. Radyushkin, Phys. Rev. D **56**, 2713 (1997) [hep-ph/9702443].

[13] M. Vanderhaeghen, M. Guidal, P. Guichon, and L. Mossé, "Computer Codes for DVCS and BH Calculations", private communications.

[14] M. Diehl *et al.*, Phys. Lett. B **411**, 193 (1997).

[15] M. Guidal, M. Garçon, E. Smith *et al.*, CEBAF experiment 99-105.

[16] P. Bertin, C. Hyde-Wright, F. Sabatié *et al.*, CEBAF experiment 00-110.

[17] M. Amarian for HERMES Coll., Deeply Virtual Compton Scattering and exclusive meson production at HERMES, talk at the workshop Skewed parton distributions and lepton-nucleon scattering, http://hermes.desy.de/workshop/TALKS/talks.html.

[18] P.R.B. Saull for ZEUS Coll., Prompt photon production and observation of Deeply Virtual Compton scattering, EPS-HEP99, Tampere 1999, hep-ex/0003030; L. Favart for H1 and ZEUS Coll., Deeply Virtual Compton Scattering at HERA, ICHEP 2000, Osaka, hep-ex/0101046.

[19] N. d'Hose *et al.*, Letter of intent to the CSTS/SPhN (2000), http://www-dapnia.cea.fr/Sphn/Vcs/Deep/.

[20] Francesca Nessi-Tedaldi, CMS conference report, presented at Beauty'97, 5th International workshop on B-Physics at Hadron machines. Los Angeles (USA), 13-17 October 1997.

[21] N. Kivel, M.V. Polyakov and M. Vanderhaeghen, Phys. Rev. D **63**, 114014 (2001); and M.V., private communication.

.